Title

Methods and instrumentation to measure the effective solar reflectance of fluorescent cool surfaces

Authors

Levinson, Ronnen
Chen, Sharon
Ferrari, Chiara
et al.

Publication Date

2017-10-01

DOI

10.1016/j.enbuild.2016.11.007

Peer reviewed

Methods and instrumentation to measure the effective solar reflectance of fluorescent cool surfaces

Ronnen Levinson[1], Sharon Chen[2], Chiara Ferrari[3], Paul Berdahl[4], and Jonathan Slack[5]

[1] Ronnen Levinson, Lawrence Berkeley National Laboratory, Berkeley, CA, USA, RML27@cornell.edu

[2] Sharon Chen, Lawrence Berkeley National Laboratory, Berkeley, CA, USA, SSChen@LBL.gov

[3] Chiara Ferrari, University of Modena and Reggio Emilia, Modena, Italy, chiara.ferrari@unimore.it

[4] Paul Berdahl, Lawrence Berkeley National Laboratory, Berkeley, CA, USA, paul.berdahl@gmail.com

[5] Jonathan Slack, Lawrence Berkeley National Laboratory, Berkeley, CA, USA, JLSlack@lbl.gov

ABSTRACT

Fluorescent cool dark surfaces stay cool in the sun by reflecting near-infrared (NIR) irradiance and by actively emitting in the NIR spectrum some of the energy absorbed from visible sunlight. The fraction of incident solar energy rejected by reflection and fluorescence is the "effective solar reflectance", or ESR, of the surface.

It is challenging to measure ESR with a solar spectrometer or a solar reflectometer, the radiometric instruments most commonly used to measure the solar reflectance (SR) of specimens in the laboratory. We have tested a variety of calorimetric techniques for using temperature in the sun to interpolate the effective solar absorptance (1 – ESR) of a fluorescent test specimen from the known solar absorptances of non-fluorescent reference specimens. Our experiments show that averaging out noise in the temperature signal induced by variations in convection is key.

We developed a computer-controlled rotary apparatus that compares the temperatures in the sun of up to six specimens. Trials on six different fluorescent specimens indicate that it can measure ESR with a repeatability of about 0.02. To maximize the ratio of signal to noise in temperature determination, and to facilitation calculation of the fluorescent benefit (ESR - SR), measurements should be performed with specimens facing the sun.

Key Words: fluorescence, effective solar reflectance, pigment, cool surface, calorimetric, rotary, spectrofluorometer, pyranometer, directionally selective reflector

1 INTRODUCTION

High solar reflectance can help keep a roof or wall cool in the sun. The coolest building envelope surfaces are bright white, reflecting about 90% of incident sunlight (spectrum 300 – 2,500 nm) when new and unsoiled (CRRC, 2016). In recent decades, cool surface designers have broadened their product color palettes by offering "cool colored" surfaces that pair low reflectance in the visible spectrum (400 – 700 nm) with high reflectance in the near-infrared (NIR) spectrum (700 – 2,500 nm). A high-performance dark cool colored surface available today, such as a natural red clay tile, may reflect about 20% of visible light, and about 60% of NIR light, to attain a solar reflectance (SR) near 0.40 (Levinson et al., 2007).

The temperature in the sun of a non-white surface can be further reduced without affecting color if the surface rapidly re-emits some of the absorbed ultraviolet (UV; 300 – 400 nm) or visible sunlight as invisible NIR radiation. These "fluorescent" cool surfaces can reject sunlight by both reflection (light leaves at the wavelength of incidence) and fluorescence (light leaves at a longer wavelength). Recent collaboration among Lawrence Berkeley National Laboratory (LBNL; Berkeley, CA, USA), PPG Industries, Inc. (Allison Park, PA, USA), and the Shepherd Color Company (West Chester, OH, USA) has yielded fluorescent cool pigments, such as ruby (Al_2O_3:Cr), that could be used to make cool dark architectural coatings (Zalich and Kornish, 2016; Berdahl et al., 2016).

The fraction of incident sunlight rejected by the combination of reflection and fluorescence is called "effective solar reflectance," or ESR. If a surface is opaque, its effective solar absorptance (ESA) α_e is one minus its effective solar reflectance ρ_e. Of course, if a surface does not fluoresce, its effective solar reflectance equals its pure solar reflectance (SR) ρ, and its effective solar absorptance equals its pure solar absorptance (SA) α.

This study examines various laboratory and field methods for measurement of ESR. We are particularly interested in techniques suited to characterize small coated specimens, on the order of 100 cm^2, that can be made from limited quantities of prototype cool fluorescent pigments.

We can classify ESR measurement techniques as radiometric (based on measuring radiation) or calorimetric (based on measuring temperature). We note that the idea of relating the solar reflectance of an opaque surface to its temperature in the sun is not new. For example, Berdahl and Bretz (1997) showed a close correlation between temperature in the sun and laboratory spectrometer measurement of solar reflectance. Also, Yuan, Emura, & Farnham (2015) used surface temperature measurements to estimate the solar reflectance of 50 cm by 50 cm samples of retroreflective building envelope materials.

2 THEORY

2.1 Calorimetric calculation of ESA and ESR

Using a standard linearization of long-wave radiative exchange, the steady-state temperature T of an adiabatic surface in the sun is governed by the energy balance

$$\alpha_e I = h_c (T - T_a) + h_r (T - T_r) , \quad (1)$$

where I is global solar irradiance (incident solar power per area); T_a is air temperature; T_r is long-wave radiative exchange temperature (equal to sky temperature, if the surface sees only the sky); and h_c is the convective heat transfer coefficient. The radiative heat transfer coefficient h_r is approximated as

$$h_r \approx 4 \varepsilon \sigma T_a^3 \quad (2)$$

where ε is surface thermal emittance and σ is the Stefan-Boltzmann constant. Solving Eq. (1) for surface temperature yields

$$T = (\alpha_e I + h_c T_a + h_r T_r) / (h_c + h_r). \quad (3)$$

This indicates that neglecting the weak temperature dependences of h_c and h_r, surface temperature will scale linearly with ESA (or with pure SA, if the surface does not fluoresce).

Consider three specimens on a common platform. If a test specimen of unknown ESA $\alpha_{e,3}$ experiences the same solar irradiance, convective heat transfer coefficient, radiative heat

transfer coefficient, air temperature, and radiative exchange temperature as nearby non-fluorescent reference specimens of known pure SAs α_1 and α_2, the ESA of the test specimen can be related to the pure SAs of the reference specimens by temperature interpolation:

$$\alpha_{e,3} = \alpha_1 + (\alpha_2 - \alpha_1)\,(T_3 - T_1) / (T_2 - T_1)\ . \tag{4}$$

The ESA of a test specimen can also be determined by fitting a line of the form

$$T = m\,\alpha + b \tag{5}$$

to the temperatures and pure SAs of the non-fluorescent reference specimens, then computing

$$\alpha_{e,3} = (T_3 - b) / m\ . \tag{6}$$

If the test specimen is opaque, its ESR will be

$$\rho_{e,3} = 1 - \alpha_{e,3}\ . \tag{7}$$

2.2 Variations with specimen position of convective heat transfer coefficient

Error in calorimetric determination of ESA via Eq. (4) may be induced by specimen-to-specimen variations in solar irradiance, thermal emittance, or convective heat transfer coefficient. Differences in solar irradiance can be minimized by keeping specimens parallel and avoiding shadows, while thermal emittance can be made consistent through choice of material. However, the forced component of the convective heat transfer coefficient can depend strongly on the distance from leading edge of the platform to leading edge of specimen. Let local Reynold's number

$$\mathrm{Re}_x = U\,x\,/\,v \tag{8}$$

where U is free-stream wind speed, x is distance from edge of plate (platform), and v is the kinematic viscosity of air. The local forced convective heat transfer coefficient

$$h_x = k\,\mathrm{Nu}_x\,/\,x \tag{9}$$

where k is the thermal conductivity of air and Nu_x is the local Nusselt number. If the flow over the plate is laminar ($\mathrm{Re}_x < 500{,}000$),

$$\mathrm{Nu}_x = 0.332\,\mathrm{Re}_x^{(1/2)}\,\mathrm{Pr}^{(1/3)} / [1 - (\xi / x)^{(3/4)}]^{(1/3)} \tag{10}$$

where Pr is the Prandtl number of air and ξ is the unheated starting length (White 1988, Eq. 6.98). If the flow over the plate is turbulent ($\mathrm{Re}_x > 500{,}000$), then

$$\mathrm{Nu}_x = (\mathrm{Nu}_x)_{\xi=0} / [1 - (\xi / x)^{(9/10)}]^{(1/9)} \tag{11}$$

where

$$(\mathrm{Nu}_x)_{\xi=0} = 0.0296\,\mathrm{Re}_x^{(4/5)}\,\mathrm{Pr}^{(1/3)} \tag{12}$$

(White, 1988, Eqs. 6.99 and 6.92).

Figure 1 shows variations with distance from leading edge of plate of laminar and turbulent local forced convective heat transfer coefficients, calculated for a free-stream wind speed of 2 m/s and zero unheated starting length. At that speed, flow is laminar ($\mathrm{Re}_x < 500{,}000$) for the first 400 cm. The laminar convective heat transfer coefficient drops rapidly from 28 W/m²·K at

1 cm, to 9 W/m²·K at 10 cm, and to 6 W/m²·K at 20 cm. This indicates that unless the specimens are centered on a large platform (say, 1 m by 1 m), variations in distance from platform edge may induce substantial specimen-to-specimen differences in temperature, and thus introduce error in calculation of ESA from measured temperatures.

2.3 Uncertainty in ESA

We can use Eq. (1) to approximate the ratio s of the uncertainty in computed ESA, $\Delta\alpha_e$, to uncertainty in measured surface temperature, ΔT, as

$$s \equiv \Delta\alpha_e / \Delta T \approx d\alpha_e / dT = (h_c + h_r) / I. \quad (13)$$

The reciprocal of this sensitivity, (1/s), can be estimated by measuring the variation with solar absorptance of the surface temperatures of non-fluorescent materials, then calculating the slope of the best linear fit to T vs. α.

3 TEST AND REFERENCE SPECIMENS

This study uses six ruby-based fluorescent test specimens prepared by some of the authors in earlier work (Berdahl et al. 2016), and 11 non-fluorescent reference specimens.

The thermal emittance of each test and reference specimen was measured with a Devices & Services Portable Emissometer following ASTM C1371-15: Standard Test Method for Determination of Emittance of Materials Near Room Temperature Using Portable Emissometers (ASTM, 2015b).

The solar spectral reflectance of each reference specimen was measured with a PerkinElmer Lambda 900 UV-VIS-NIR spectrometer with 150 mm Labsphere integrating sphere, following ASTM E903-12: Standard Test Method for Solar Absorptance, Reflectance, and Transmittance of Materials Using Integrating Spheres (ASTM, 2012). Each specimen was mounted at the sphere's reflectance port in the conventional manner to measure "without window" solar spectral reflectance. In some cases, it was also measured with a quartz window between the port and the specimen to determine "with window" solar spectral reflectance. Each solar spectral reflectance was weighted with an air mass 1 global horizontal (AM1GH) solar spectral irradiance to calculate AM1GH solar reflectance (Levinson, Akbari, & Berdahl, 2010a,b).

The pure solar reflectance each test specimen was measured in accordance with Section 4.2, below.

3.1 Fluorescent test specimens

The first test specimen, "ruby crystal clear", is a clear-coated ruby crystal array on a white substrate (Figure 2a). Each crystal is a square pyramid, approximately 5 mm by 5 mm by 2.6 mm. The clear acrylic increases the thermal emittance of this specimen to 0.875 from 0.765 for uncoated crystals.

The remaining five fluorescent test specimens are ruby-pigment coatings (Figure 3). Each coating was prepared by mixing ruby pigment (alumina doped with chromium oxide) into clear acrylic, then applying the pigmented acrylic to bright white substrate (an aluminum panel painted white). The ruby-pigment coatings are labelled 0.2%, 1%, 2%, 3%, and 4% according to the weight fraction of chromium oxide (Cr_2O_3) present in the alumina (Al_2O_3) pigment. Their thermal emittances range from 0.876 to 0.885 (Table 1).

3.2 Non-fluorescent reference specimens

We prepared 11 non-fluorescent reference specimens, each 75 mm by 75 mm (Table 2). References specimens A1 – A9 are aluminum panels hand painted with two layers of titanium oxide white, then overcoated with titanium oxide white and/or bone black to create a white, gray, or black surface (Figure 4). Their thermal emittances range from 0.886 to 0.926.

Reference specimen A10, “ruby crystal white”, is an aluminum panel with a ruby crystal array, overpainted white (Figure 2c); reference specimen A11, “ruby crystal gray”, is the analog of specimen A10, but overpainted gray, rather than white (Figure 2a). Their thermal emittances are 0.911 and 0.912, respectively. Ruby crystal white and ruby crystal gray each have essentially the same shape and thermal properties as ruby crystal clear.

4 RADIOMETRIC MEASUREMENT OF ESR

4.1 Spectrofluorometer

Absolute and complete spectral fluorescence measurements are not routine, so complete calibrated measurements are uncommon. However, measurement of spectral emission intensity (arbitrary units) is essential for optimizing fluorescent materials. One can compare emission from various samples under the same conditions to find the spectral distributions and even small differences in intensity.

LBNL adapted equipment formerly used to determine the albedo of polluted snow (Hadley & Kirchstetter, 2012) to make a spectrofluorometer that measures fluorescence over the spectrum 500 – 1,100 nm. The apparatus includes a tungsten lamp (with xenon gas fill), a high-quality short-pass filter (optical density 4) to block wavelengths that would interfere with observation of the fluorescence emission, a 150 mm Labsphere integrating sphere, and a spectrophotometer. The incident light passes through the integrating sphere to strike the fluorescent sample, and the diffuse emission is collected by the integrating sphere. An optical fiber port on the sphere passes the fluorescence to the input fiber of a compact Ocean Optics S2000 spectrometer with a fixed diffraction grating and a silicon array detector. The fluorescence spectra of several ruby coatings are shown range at full scale in Figure 5 and with greater detail in ESM Figure A-1.

PPG purchased a PTI (Photon Technology International) QM-500 spectrofluorometer that uses an InGaAs detector (500 – 1,700 nm). The instrument determines the excitation wavelength with an input monochromator and the emission wavelength with an output monochromator, and can thus determine both excitation and emission spectra. This arrangement is more sensitive at longer wavelengths, while the LBNL fluorescence instrumentation, using a silicon array detector, is insensitive to radiation beyond about 1,100 nm.

Since measurements from each spectrofluorometer are reported in arbitrary units, neither instrument can be used as configured to assess effective spectral reflectance (ratio of emitted + reflected power to excitation power, as a function of excitation wavelength). However, it may be possible to adapt the PTI QM-500 spectrofluorometer to measure effective spectral reflectance by calibrating its input (excitation) and output powers, and adding an integrating sphere. The same adapted spectrofluorometer could also be used to measure pure spectral reflectance by measuring output power only at the excitation wavelength.

4.2 Spectrophotometer

Using a UV-VIS-NIR spectrophotometer with integrating sphere to measure effective spectral reflectance is not feasible, because the instrument’s calibration protocol assumes that the

wavelength of detected light is the same as that of incident light. The effective reflectance spectrum will be inaccurate if instrument response at emission wavelengths differs from that at excitation wavelengths. However, this apparatus can be used to measure the pure spectral reflectance of a fluorescent surface by selectively filtering its detector(s). Pure spectral reflectance can be used to calculate pure solar reflectance, which in turn can be subtracted from ESR to assess the portion of ESR attributable to fluorescence.

For example, ruby emits in the spectrum 650 – 800 nm, with strong peaks near 694 nm (edge of visible spectrum). Covering the photomultiplier used to detect 250 – 900 nm radiation with a filter that blocks this emission (ESM Figure A-2) permits measurement of pure spectral reflectance from 250 to 650 nm. Pure spectral reflectance over the remainder of the solar spectrum (650 – 2,500 nm) can be measured without a filter, since incident radiation at these wavelengths does not excite ruby. Figure 6 shows the apparent solar spectral effective reflectance (blue curve) and the solar spectral pure reflectance (red curve) of ruby crystal clear. Using an air mass 1 global horizontal (AM1GH) solar spectral irradiance to compute broadband properties (Levinson, Akbari, & Berdahl, 2010a,b), the apparent difference between apparent effective solar reflectance (0.452) and pure solar reflectance (0.434) is only 0.017. We will later demonstrate that the true ESR of this specimen is about 0.74, indicating that the apparent ESR assessed by spectrophotometer was about 0.28 low.

4.3 Reflectometer

Using the Solar Spectrum Reflectometer (Devices & Services, Dallas, TX, USA) to measure ESR presents a similar challenge, because its calibration protocol also assumes that the wavelength of detected light is the same as that of incident light. For example, using version 6 of this instrument to measure the AM1GH ("G1") solar reflectance of ruby crystal clear yields 0.508, or about 0.22 below true ESR. We also note that the incandescent lamp in this reflectometer may not generate enough UV light to excite certain fluorescent pigments.

4.4 Pyranometer

The ESR of a very large specimen (at least 4 m by 4 m) could be measured with a first-class pyranometer following ASTM E1918-06(2015): Standard Test Method for Measuring Solar Reflectance of Horizontal and Low-Sloped Surfaces in the Field (ASTM, 2015a). Specifically, E1918 could yield ESR as the ratio of the reflected and fluoresced upflux measured by a downward-facing pyranometer to the solar irradiance measured by an upward-facing pyranometer.

The ESR of a large specimen (about 1 m by 1 m) could be measured with a first-class pyranometer following non-ASTM method E1918A (Akbari, Levinson, & Stern, 2008; Levinson, Akbari, & Berdahl, 2010b). The E1918A technique exactly covers a test surface with a stacked pair of opaque, non-fluorescent masks of known solar reflectance. The lower mask is black and the upper mask is white. A downward-facing pyranometer first measures upflux with the white mask exposed. The white mask is removed, and upflux is remeasured with the black mask exposed. The black mask is removed, and the upflux is measured a third time with the test surface exposed. The ESR of the test surface can be interpolated from the SRs of the white and black masks by comparing the upflux with test surface exposed to the upfluxes with white and black masks exposed.

Since neither E1918 nor E1918A can determine the ESR of a small test specimen (about 10 cm by 10 cm), these techniques will be more useful when fluorescent cool envelope materials are available in large quantities.

4.5 Pyrheliometer plus pyranometer

The ESR of a small test specimen could be measured by using a pyrheliometer to measure reflected plus fluoresced upflux, and a pyranometer to measure downflux (solar irradiance). ESR could then be calculated as the ratio of the measured upflux to the product of the measured irradiance and the view factor from the pyrheliometer to the portion of the test surface that it sees.

The challenge is that since a pyrheliometer has a narrow field of view, it would measure a very small upflux from a test surface whose reflection and fluorescence are diffuse. For example, a vertical pyrheliometer with a 38 mm diameter collimating tube and a 1° "slope" angle that is placed 100 mm above a test surface would see a target of diameter 41 mm. The view factor from the detector tube opening to the target would be 0.039. If the test surface receives an irradiance of 1000 W/m² and has an ESR of 0.50, the pyrheliometer would measure an upflux of 19.5 W/m². Raising ESR by 0.05 would increase the measured upflux by only 2 W/m², suggesting that the signal to noise ratio of ESR measurement could be small.

As an aside, it would be reasonable to consider the use of a pyranometer or pyrheliometer plus pyranometer to determine ESR as calorimetric, since each instrument measures radiance with a thermopile. We choose to classify them as radiometric because these methods calculate ESR from radiances, rather than temperatures.

5 EXPERIMENTS TO DESIGN CALORIMETRIC APPARATUS

The following series of experiments was used to design and refine techniques for calorimetric assessment of ESR in accordance with Eqs. (4) through (7).

5.1 Experiment 0A: Measuring ESA of ruby crystal clear exposed on reclining chair

The temperature in the sun of ruby crystal clear was compared to those of three reference specimens: A10 (ruby crystal white), A1 (white), and A2 (gray#1). The support was the adjustable back of a reclining chair facing directly into the sun. A light beige towel was placed under the samples and over the chair's upholstered pad (ESM Figure A-3). The four specimens were laid out with 25 mm gaps along the width of the pad (560 mm), leaving about 90 mm of pad on each side of the array.

The temperature of the back of each specimen was measured with a thermistor and recorded with a data logger, as detailed in ESM Table A-1. The trial began about 13:00 local daylight time (LDT) on 2015-06-23 in Walnut Creek, CA, USA (clear sky, air temperature 31.6 °C, slight breeze). After a 15 minute warm up, an 11 minute period with fairly steady temperatures was chosen for analysis.

Two determinations of ESA for the ruby crystal sample were performed. Simple temperature interpolation with A1 (white) and A2 (gray #1) yielded an ESA of 0.262, which is close to that of A2 (0.267). However, since the convective heat transfer coefficient over the ruby crystal array might differ from that over a smooth painted metal panel, the ESA of the test specimen was also extrapolated from that of ruby crystal white, as follows. The ruby crystal sample was about 2.4 °C warmer than ruby crystal white (SA 0.231). We calculated the convective heat transfer coefficient over the ruby crystal white specimen by assuming I = 1050 W/m², h_r = 6 W/m²·K, and $T_r = T_a - 12$ °C, then solving Eq. (1) to obtain h_c = 9 W/m²·K. Using this convective heat transfer coefficient for ruby crystal clear, Eq. (1) was solved to find ρ_e = 0.264. The mean of the two determinations was 0.263, and thus the ESR is 0.737.

5.2 Experiment 0B: Assessing linearity of surface temperature vs. ESA with nine reference specimens exposed on reclining chair

To test the linear relationship between surface temperature and ESA required for use of Eq. (4), the temperatures of the nine painted metal reference specimens (A1 – A9) were measured at the same site and using the same support (reclining chair back plus towel) used in Experiment 0A. The nine specimens were arranged in a three by three array with about 2.5 cm spacing. The top three samples were A1 – A3, with A4 – A6 in the middle, and A7 – A9 at bottom. The left and right margins were each about 14 cm.

On 2015-07-28 at 13:45 LDT (clear sky, air temperature 40 to 40.5 °C, calm), the specimens were placed on the support to warm up for 25 min. Their upper surface temperatures were then measured with an infrared thermometer eight times over the next 30 min, as detailed in ESM Table A-1. Median surface temperature varied nearly linearly with solar absorptance (Figure 7), supporting use of Eq. (4). The slight downward curvature in this plot is likely due to slight increases in the radiative and convective heat transfer coefficients with increasing temperature.

5.3 Experiment 1: Measuring ESA of ruby crystal panel exposed on three-specimen platform

With the goal of creating a simple portable apparatus for reproducible calorimetric measurement of ESA, we built a 15 cm by 30 cm by 5 cm platform from white foam board (lightweight moisture-resistant low density polystyrene) with three specimen cavities, each 76 mm by 76 mm (Figure 8). Each cavity can support an optional quartz window (100 mm by 100 mm by 1.6 mm) above the specimen to reduce wind noise. A silicon pyranometer measures solar irradiance, while a handheld vane anemometer is used to measure wind speed. Thermistors were affixed to the back of each specimen with thermal paste and aluminum tape, as detailed in ESM Table A-1.

We made three versions of this platform, each with a uniform cavity depth of 6 mm (0.25”), 13 mm (0.5”), or 19 mm (0.75”). Trials were conducted at LBNL at various times between 10:50 and 15:40 LDT on sunny days in September 2015. In each trial, the test specimen was the ruby crystal array with clear overcoat. One reference specimen was always A1 (white), and the second was either A2 (gray#1) or A3 (gray#2). The platform was oriented to face the sun (surface normal parallel to solar beam).

Figure 9 shows five different trials in which test specimen ESA was calculated from Eq. (4). The horizontal line shows the ESA measured in Experiment 0A (0.263). Trial 1A, using no window and the shallowest (6 mm) cavity, yielded an ESA only about 0.01 lower than that found in Experiment 0A, but with noticeable wind noise. Adding windows (trial 1B) further lowered the estimate of ESA by about 0.06 without reducing noise. Retaining windows while increasing cavity depth to 13 mm (trials 1C and 1E) or 19 mm (trial 1F) eliminated window noise, but yielded ESAs about 0.02 to 0.03 lower than found in Experiment 0A.

5.4 Experiment 2: Measuring surface temperatures of non-fluorescent specimens on five-specimen platform

To explore the effects of wind-induced surface temperature fluctuations measured without protective windows, we measured the temperatures of non-fluorescent metal specimens on several different platforms. Six trials, 2A – 2F, were conducted at LBNL on sunny but often windy days in October 2015, between 11:40 and 16:00 LDT. Trials 2A – 2C exposed a set of five duplicate 50 mm by 50 mm green specimens (SA 0.88), while trials 2D – 2F tested a set of five different 50 mm by 50 mm specimens (SAs 0.72, 0.73, 0.77, 0.88, 0.96).

Trial 2A arranged the five duplicate specimens in two rows at the center of a 36 cm by 38 cm by 2.5 cm foam board; Trial 2B arranged them in one row on a 20 cm by 61 cm by 2.5 cm foam board; and Trial 2C set them in a cavity array (9 cm by 9 cm, 25 mm deep). Trial 2D exposed the five different specimens as in Trial 2B; Trial 2E added a parapet-style wind break (25 mm height, 5 cm from the specimen row) to the Trial 2D setup; and Trial 2F exposed these five different specimens exposed as in Trial 2C (ESM Figure A-4).

The platform was oriented to face the sun. After a 10 minute warm up, specimen temperatures were recorded every 10 seconds for a period of 20 minutes.

Trials 2A – 2C yielded temperature range (max – min) values of about 1 to 2 °C. Trials 2D – 2F yielded surface temperatures that generally increased with solar absorptance, but with much more noise and less linearity than observed on a calm day in Experiment 0B (Figure 7).

The slopes of the lines fit to T vs. α in Figure 7 range from 31.4 to 42.1 °C per unit change in solar absorptance. We can use these slopes to relate error in ESA to error in measured surface temperature. For example, in Experiment 0B or Experiment 2D, an error of 1 °C would change ESA by 0.027.

5.5 Experiment 3: Measuring surface temperatures of non-fluorescent specimens on rotating apparata (early versions)

Since specimen placement, especially distance from leading edge of platform to specimen, is expected to affect convective heat transfer coefficient, surface temperature, and finally estimation of ESA, we tried symmetrically arranging duplicate specimens on a rotating platform to make convection more uniform.

Our first approach manually rotated the square platform (33 cm by 33 cm by 2.5 cm) shown in ESM Figure A-5, which faced the sun. Trials 3A and 3B were conducted at LBNL on sunny afternoons in November 2015. Following a 10 minute warm up, each trial rotated the platform a quarter turn every 5 min for 20 minutes, with a data logger recording specimen temperatures every 10 seconds. At the end of trial 3A, the time-averaged temperature range was 1.1 °C; at the end of trial 3B, it was 0.4 °C (ESM Figure A-6).

Our second approach installed a circular platform of diameter 30 cm on the platter of a phonographic turntable (Figure 10). The platform was horizontal and revolved at 0.55 Hz (33 RPM). As in previous trials, the specimens were allowed a 10 minute warm up period. In trial 3C, conducted at LBNL on a sunny, calm late morning in January 2016, the time-averaged temperature range over a 6 minute measurement period was 0.4 °C (Figure 11).

5.6 Experiment 4: Measuring surface temperatures of non-fluorescent specimens on first programmable rotating platter

We built a rotating platter that holds six specimens, and positions each in turn under a fixed infrared thermometer. The first version of this programmable apparatus measured the temperature of each specimen for several seconds, recorded the final value, then quickly rotated the platter to bring the next specimen into the thermometer's narrow field of view.

The platter, a 5.1 cm thick, 45 cm diameter slab of expanded polystyrene (EPS) foam adhered to a thin aluminum plate, was rotated by a computer-controlled electric stepper motor. The angular position of the platter was continuously measured with a shaft-mounted goniometer to provide closed-loop control of platter rotation. Up to six specimens, each 50 to 75 mm on a side, could be placed at 60° intervals on the surface of the platter, which in turn was faced into the sun (ESM Figure A-7). The operator could specify (a) the duration and speed of pre-measurement "spin-up" revolutions; (b) the number of measurement revolutions; (c) the

duration of each temperature measurement; and (d) the speed with which to rotate the platter to bring the next specimen under the thermometer.

We conducted four trials, 4A – 4D, in April 2016. In each trial, the platter was spun at 30 RPM for 10 minutes to minimize any pre-trial differences in specimen temperature that might result from spatial variations in convection coefficient or solar irradiance. Next, over a series of 20 to 40 revolutions, the platter was rotated in increments of 60° to bring each specimen under the thermometer. Specimen temperature was recorded after 4 to 5 seconds of measurement. The platter was then rotated for about 2 sec to bring the next specimen into view.

Trials 4A and 4B exposed six duplicate green specimens—the same as those used in Experiments 2 and 3—on April 15 (sunny) and April 18 (intermittently cloudy, and windier), respectively. Trial 4B temperature and solar irradiance time series are shown in ESM Figure A-8. Trial 4A yielded time-averaged temperatures with a range of 0.18 °C after 40 revolutions, while Trial 4B yielded a range of 0.74 °C after 35 revolutions (ESM Figure A-9).

Trials 4C and 4D exposed reference specimens A1 (white), A2 (gray #1), A3 (gray #2), A4 (gray #3), A7 (gray #6), and A9 (black) on April 15 and April 18, respectively. Trial 4D temperature and solar irradiance time series are shown in Figure 12. While instantaneous temperatures fluctuated over the course of each trial, time-averaged surface temperatures varied linearly with solar absorptance (Figure 13).

5.7 Upgrading the programmable rotating platter to create final apparatus

After Experiment 4, we improved the capabilities and performance of the programmable rotating platter by changing its drive motor, expanding its suite of local weather sensors, and upgrading its electronics and control software. These improvements made it substantially easier to operate the apparatus and to use its measurements to assess ESR.

First, we smoothed the rotation of the platter by replacing its stepper motor drive with a variable-speed DC motor drive. This reduced the tendency of the platter to vibrate when its motion is halted, and increased the accuracy with which each specimen can be positioned below the IR thermometer. Second, we added a three-cup anemometer to measure local wind speed, and a shaded thermistor to measure ambient air temperature. Third, we replaced the handheld data logger with a computer-controllable, multifunction data acquisition (DAQ) device. This increased the accuracy of sensor signal digitization and made all measurements immediately available to the apparatus control software. Fourth, we upgraded the control software (Python code executed on a Windows PC) to (a) better regulate the motion of the platter; (b) capture specimen temperature, weather, and platter angle at the end of each specimen measurement; and (c) record to a file the time-stamped instantaneous specimen temperature and weather measurements, along with cumulative mean specimen temperatures, as they are captured.

The final apparatus is shown in Figure 14 and detailed in ESM Table A-1. A video of the platter motion is online at https://goo.gl/CdLOzE .

6 MEASUREMENT OF ESR WITH FINAL APPARATUS

In Experiment 5 (September 2016), we used the final apparatus to measure the ESRs of ruby crystal clear and the five fluorescent ruby-pigment coatings.

6.1 Methodology

We conducted 30 trials at LBNL with the upgraded apparatus in late September 2016. The fluorescent specimens were grouped with non-fluorescent reference specimens to form four

test sets (A – D). Set A compared the 0.2%, 1%, and 2% coatings to references A1 (white), A2 (gray#1), and A3 (gray#2), while Set B compared the fluorescent 2%, 3%, and 4% coatings to the same three references. Note that the 2% coating was present in both Set A and Set B.

Set C compared ruby crystal clear to references A10 (ruby crystal white) and A11 (ruby crystal gray). Set D was Set C plus the 2% coating and references A1 (white) and A2 (gray#1) (Figure 15). Set E, comprised of references A1 (white), A2 (gray #1), A3 (gray#2), A4 (gray#3), A7 (gray#6), and A9 (black) was measured to verify that the reference temperatures varied linearly with solar absorptance.

Sets A, B, and C were tested facing the sun in trials 5A – 5C, 5D – 5F, and 5G – 5I, respectively, then tested horizontally with solar elevation angles of 45 to 52° in trials 5J – 5L, 5M – 5O, and 5P – 5R. Set D was tested horizontally in extended trial 5S, a series of 10 subtrials (5S/i through 5S/x) in which the solar elevation angle ranged from 18° to 49°. Set E temperatures were measured facing the sun in trial 5T, then horizontally in trial 5U.

Each trial included a 10 min spin up at about 8 RPM, except in extended trial 5S, where spin-up time was reduced to 1 min when the gap between consecutive subtrials was less than 10 min. With the exception of Trial 5U, which was briefer, each trial (or subtrial) included about 25 to 50 measurement revolutions (Table 3). In the measurement phase, the apparatus held each specimen under the IR thermometer for 5 seconds before spinning the platter at about 6 RPM to bring the next specimen into view.

The ESA and ESR of each specimen was calculated following Eqs. (5) through (7).

6.2 Results

Figure 16 illustrates the output of the apparatus with the time series of solar irradiance, wind speed, air temperature, and instantaneous and cumulative mean specimen temperatures measured in Trial 5C.

Figure 17 shows how the ESA of each fluorescent test specimen in trials 5D – 5F was determined by locating its final mean temperature on a line fit through the final mean temperatures and pure SAs of the non-fluorescent references. Similar plots for all trials involving fluorescent specimens (5A – 5R) are presented in ESM Figure A-10.

Specimen ESRs are reported by trial in Table 3 and summarized in Table 4. Mean ESR measured horizontally was 0.047 higher than mean ESR measured facing the sun for ruby crystal clear, and 0.021 to 0.031 higher for the coatings. For a given specimen and orientation, ESR sample standard deviation ranged from 0.002 to 0.023.

The variations with solar beam incidence angle of the ESRs of the 2% coating and of ruby crystal clear are shown in Figure 18.

The linear variation with pure SA of the final mean temperatures of non-fluorescent reference specimens is shown in ESM Figure A-11.

7 DISCUSSION

7.1 Radiometric measurement techniques

Two of the radiometric ESR measurement techniques (pyranometer methods E1918, requiring a sample at least 4 m by 4 m; and E1918A, requiring a sample about 1 m by 1 m) are promising for rating commercial products once available at large scale, but not for measuring the ESR

of small prototype specimens (10 cm by 10 cm). The combination of a pyrheliometer and pyranometer may work to characterize small specimens if the ratio of signal to noise can be improved.

It may be possible to calibrate the input and output of a spectrofluorometer to provide absolute measurement of the effective spectral reflectance of a small specimen. Such an instrument would not have to cover the entire solar spectrum so long as it includes all excitation and emission wavelengths. Pure reflectance at non-excitation wavelengths could be assessed with a traditional spectrophotometer.

7.2 Calorimetric measurement techniques

From the calorimetric measurement design experiments we draw the following observations.

1. Specimen surface temperature varied nearly linearly with SA on a calm, sunny day, validating the calculation of ESA by temperature interpolation of known SA values (Experiment 0B).

2. ESA can be measured in calm, sunny conditions (Experiment 0A).

3. Wind can induce variations of about 2 °C in duplicate specimen surface temperature if the specimens are stationary and unshielded (Experiment 2).

4. Shielding specimens with a window removes convection noise, but yields ESA different from that measured with unshielded specimens on a calm, sunny day (Experiment 1).

5. Rotating the specimen platform and averaging the time series of specimen temperature measurements mitigates convection noise (Experiments 3 through 5).

Experiments 3 through 5 identified two useful rotary techniques: (a) continuous measurement of the temperature of each specimen with a contact thermometer, such as a thermistor, thermally connected to its back; and (b) intermittent measurement of the temperature of each specimen with a single IR thermometer that sees each specimen in turn. Each has practical advantages and disadvantages.

Continuous measurements can be recorded with a small, standalone logger, so long as the logger can revolve with the platter. No computer control is required, since the platter can spin at a constant speed. Weather measurements can be collected with a second logger. The primary disadvantages to this method are that (a) the temperature sensors must be cross calibrated, ideally before each trial; (b) the temperature sensors must be joined to specimens with thermal paste to minimize thermal resistance; (c) this thermal resistance may grow if the sensor is dislodged; and (d) a standalone logger that can record and process thermistor and pyranometer signals tend to be expensive (about US$1K). The first three issues can be managed. For example, one could use thermal epoxy, rather than thermal paste, to permanently bond an accurate but inexpensive thermistor (example: US Sensor KS103G2, 0.1 °C interchangeability, US$5) to the back of each specimen, then cross-calibrate the sensors by measuring specimen temperatures in the dark. As for the last issue, we note that the labor savings associated with this simple design may offset the investment in data logging equipment.

Intermittent measurements can be performed with a single, non-contact IR thermometer, removing the needs to cross calibrate multiple temperature sensors and thermally bond them to the specimens. This makes it easy to change specimens. Computer control of platter motion and data collection makes the system programmable and versatile, and analysis features built into the control software reduce the need to post-process temperature measurements. On the

other hand, even when the broadband thermal emittances of specimens are matched, the use of an IR thermometer can complicate assessment of surface temperature if there are specimen-to-specimen variations in spectral emittance within the portion of the thermal IR detected by the sensor (Micro-Epsilon 2016).

The intermittent-measurement apparatus is more complicated than that needed for continuous measurement. Substantial effort was required to design and build the electronics and software needed to intermittently rotate the platter, synchronize temperature measurements to platter motion, and communicate with the DAQ hardware. We note in particular that early attempts to use an inexpensive hobbyist microcontroller with integrated analog and digital I/O uncovered serious limitations in such microcontrollers, including limited range and resolution of analog input; lack of basic functionality, such as a battery powered clock to maintain system time; and incomplete, unsupported application program interfaces for both the microcontroller and its accessories, such as external analog-to-digital conversion integrated circuits. We resolved these problems by switching to a more expensive, but more robust, scientific-grade DAQ device.

7.3 ESR measurement repeatability and technique

The Experiment 5 trials indicate that the final apparatus measures the ESR of a given specimen, in a given orientation, with a repeatability (sample standard deviation) of about 0.02.

In our earliest experiments with a clear-coated ruby array with sun normal to the sample, we found ESR = 0.737. At the conclusion of the present work we have ESR = 0.764. The difference, 0.027, is within the combined uncertainties of the two measurements and is indicative of the current state of the art. On the other hand, under favorable circumstances, the standard deviations (repeatability) obtained with the current apparatus is as small as 0.002, so there is room for further improvement.

The ESR of the ruby crystal clear was about 0.05 higher measured horizontally (solar incidence angle around 50°) than when measured facing the sun. This may result from variations with beam incidence angle in specular reflectance from the clear-coated crystals. (The white- and gray-coated crystals appear matte.) A normally incident photon must be reflected twice before leaving the pyramid surface of the ruby crystal array, reducing net reflectance. For example, if the sloping top surface reflectance of a ruby crystal is 0.07, the net surface reflectance for a normally incident photon is only $0.07 \times 0.07 = 0.0049$. For incidence angles well away from normal incidence the surface reflectance should be comparable to 0.07.

The ESR of the coatings was about 0.02 higher measured horizontally (solar incidence angle around 50°) than when measured facing the sun. The reason for this variation is unclear, but is not surprising since reflectance often increases with incidence angle (Appendix A of Levinson, Akbari, and Berdahl 2010a).

We recommend measuring ESR with specimens facing the sun, for three reasons. First, since pure solar reflectance is typically measured at near-normal incidence, measuring ESR at normal (or near normal) incidence makes it easier to compute the fluorescence benefit (ESR – pure SR). Second, facing the sun provides a consistent incidence angle. Third, facing the sun maximizes the incident solar flux, increasing the ratio of signal (temperature rise induced by solar heat gain) to noise (temperature fluctuations induced by variations in convection).

7.4 Other applications

Our calorimetric technique could also be applied to other special surfaces, including directionally selective reflectors (DSRs) used as cool envelope materials. The solar reflectance of a DSR, such as a retroreflector, or a roofing product that looks white from the sky and dark from ground level, is inconvenient to measure with a conventionally configured spectrophotometer that provides only near-normal irradiance. It could be measured at any solar incidence angle using our calorimetric technique, though measurement at incident angles approaching 90° may substantially reduce the ratio of signal-to-noise.

8 SUMMARY

Test methods are needed to evaluate the abilities of surfaces colored with fluorescent cool pigments to reject incident sunlight by the combination of reflection and fluorescence. Our review of radiometric techniques for the measurement of effective solar reflectance suggests that two pyranometer methods (E1918A, E1918) could be applied to large or very large specimens, and that a suitably calibrated spectrofluorometer fitted with an integrating sphere could measure the effective spectral reflectance of a small specimen.

We have tested a variety of calorimetric techniques for using temperature in the sun to interpolate the effective solar absorptance of a test specimen from the known solar absorptances of non-fluorescent reference specimens. Our experiments showed that averaging out noise in the temperature signal induced by variations in convection is key.

We have developed a computer-controlled rotary apparatus that compares the temperatures in the sun of up to six specimens. Trials on six different fluorescent specimens indicate that it can measure ESR with a repeatability of about 0.02. To maximize the ratio of signal to noise in temperature determination, and to facilitation calculation of the fluorescent benefit, measurements should be performed with specimens facing the sun.

This apparatus could also be used to assess the solar reflectance of directionally selective reflectors that are difficult to characterize with conventional laboratory instruments.

ACKNOWLEDGEMENTS

This work was supported by the Assistant Secretary for Energy Efficiency and Renewable Energy, Office of Building Technology, State, and Community Programs, of the U.S. Department of Energy under Contract No. DE-AC02-05CH11231; and by the California Energy Commission (CEC) through its Electric Program Investment Charge (EPIC). We also wish to thank Howdy Goudy of Lawrence Berkeley National Laboratory for assistance with electronics; Katerina Tsou of Michigan State University for her contributions to measurements; and Victor Cassella of Kipp & Zonen for loan of an SP Lite2 pyranometer.

REFERENCES

Akbari, H., Levinson, R., & Stern, S. (2008). Procedure for measuring the solar reflectance of flat or curved roofing assemblies. *Solar Energy*, 82, 648-655.

ASTM. (2012). ASTM E903-12: Standard Test Method for Solar Absorptance, Reflectance, and Transmittance of Materials Using Integrating Sphere. ASTM International. http://www.astm.org/Standards/E903.htm

ASTM. (2014). ASTM C1549-09(2014): Standard Test Method for Determination of Solar Reflectance Near Ambient Temperature Using a Portable Solar Reflectometer. http://www.astm.org/Standards/C1549.htm

592 ASTM. (2015a). ASTM E1918-06(2015): Standard Test Method for Measuring Solar
593 Reflectance of Horizontal and Low-Sloped Surfaces in the Field. ASTM International.
594 http://www.astm.org/Standards/E1918.htm

595 ASTM. (2015b). ASTM C1371-15: Standard Test Method for Determination of Emittance of
596 Materials Near Room Temperature Using Portable Emissometers. ASTM International.
597 http://www.astm.org/Standards/C1371.htm

598 Berdahl, P. and Bretz, S. (1997). Preliminary survey of the solar reflectance of cool roofing
599 materials. *Energy & Buildings*, 25, 149-158. Figures 11, 12.

600 Berdahl, P., Chen, S. S., Destaillats, H., Kirchstetter, T. W., Levinson, R.M., & Zalich, M. A.
601 (2016). Fluorescent cooling of objects exposed to sunlight – the ruby example. *Solar Energy*
602 *Materials & Solar Cells* 15, 312–317.

603 CRRC. (2016). Rated Products Directory, Cool Roofing Rating Council, Oakland, CA, USA.
604 http://coolroofs.org

605 Hadley, O. L., & Kirchstetter, T. W. (2012). Black-carbon reduction of snow albedo, *Nature*
606 *Climate Change*, 2(6), 437-440.

607 Levinson, R., Akbari, H., & Berdahl, P. (2010a). Measuring solar reflectance—Part I: defining
608 a metric that accurately predicts solar heat gain. *Solar Energy*, 84, 1717-1744.

609 Levinson, R., Akbari, H., & Berdahl, P. (2010b). Measuring solar reflectance—Part II: review
610 of practical methods. *Solar Energy*, 84, 1745-1759.

611 Levinson, R., Berdahl, P., Akbari, H., Miller, W., Joedicke, I., Reilly, J., Suzuki, Y., &
612 Vondran, M. (2007). Methods of creating solar-reflective nonwhite surfaces and their
613 application to residential roofing materials. *Solar Energy Materials & Solar Cells*, 91, 304-
614 314.

615 Micro-Epsilon. 2016. Basics of Non Contact Temperature Measurement. Document
616 Y9766331-A021021DGO, Micro-Epsilon, Rayleigh, North Carolina, USA. Retrieved on 2016-
617 10-03 from http://www.micro-epsilon.com/download/products/dat--infrared-basics--en-us.pdf
618 .

619 White, F. M. (1988). *Heat and Mass Transfer*. Addison-Wesley.

620 Yuan, J., Emura, K., & Farnham, C. (2015). A method to measure retro-reflectance and
621 durability of retro-reflective materials for building outer walls. *Journal of Building Physics*,
622 38(6), 500–516.

623 Zalich, M., & Kornish, B. (2016). Fluorescent pigments for high-performance cool roofing and
624 facades. PPG Industries. Research Performance Progress Report (RPPR) for DOE/EERE,
625 Award DE-EE0006347. Submitted to http://osti.gov .

626

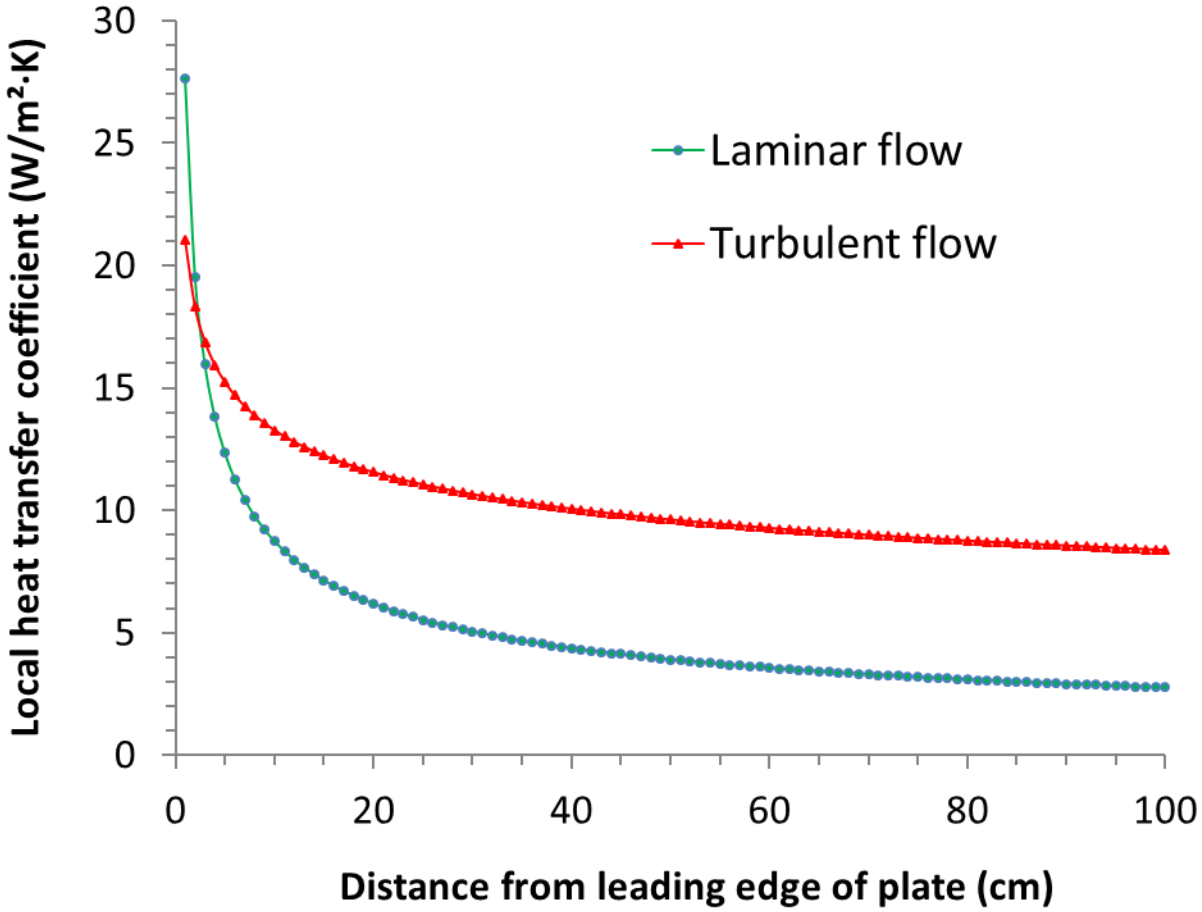

Figure 1. Variations with distance from leading edge of plate of laminar and turbulent local forced convective heat transfer coefficients, calculated for a free-stream wind speed of 2 m/s. At that speed, flow is laminar (local Reynold's number < 500,000) for the first 400 cm.

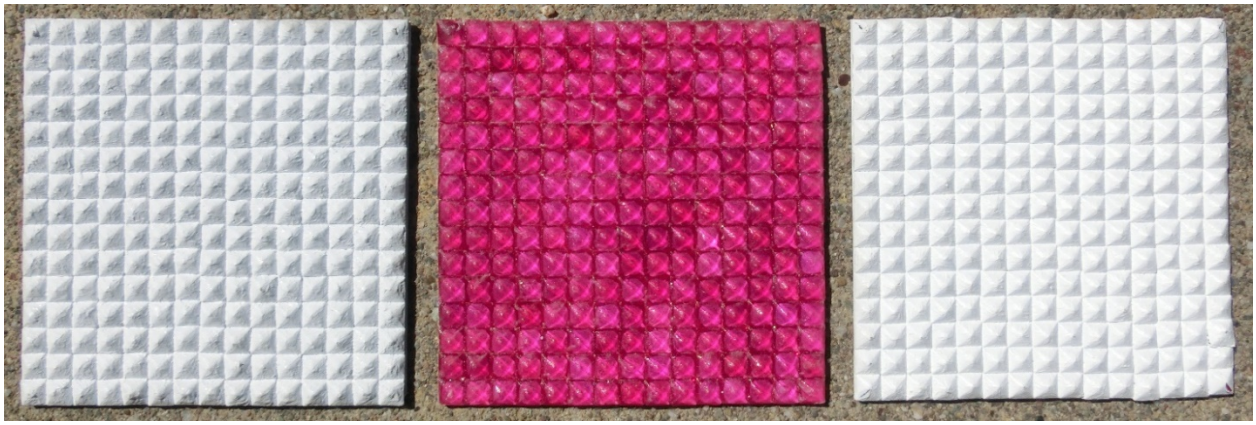

Figure 2. Images of 75 mm by 75 mm ruby crystal specimens overcoated with (a) gray acrylic paint (“ruby crystal gray”), (b) clear acrylic paint (“ruby crystal clear”), or (c) white acrylic paint (“ruby crystal white”). The gems are set in a thick layer of bright white artist paint on an aluminum substrate.

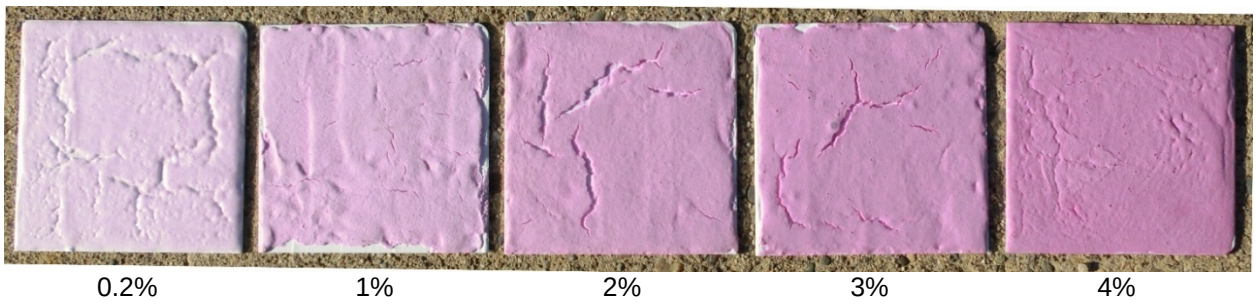

Figure 3. Images of 75 mm by 75 mm ruby-pigment coatings with 0.2%, 1%, 2%, 3%, or 4% weight fractions of chromium oxide present in the alumina pigment.

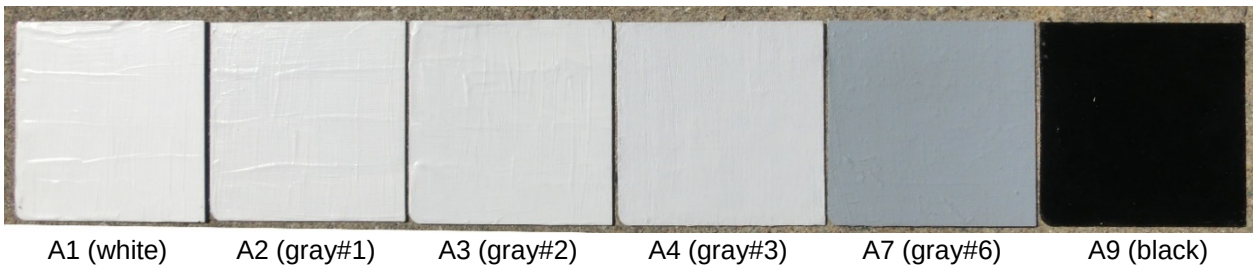

Figure 4. Images of six of the painted metal panels (A1 – A9) used as non-fluorescent reference specimens: A1 (white), A2 (gray#1), A3 (gray#2), A4 (gray#3), A7 (gray#6), and A9 (black). Each panel is 75 mm by 75 mm.

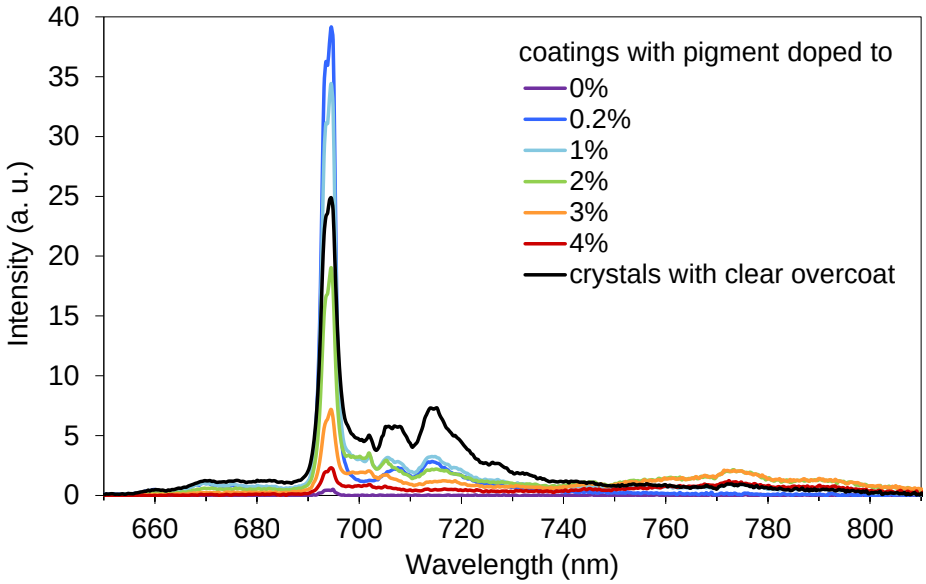

Figure 5. Fluorescence spectra obtained with the LBNL spectrofluorometer of highly-pigmented ruby coatings with ~500 g m^{-2} of 0 to 4 wt% Cr_2O_3-doped Al_2O_3, and of the ruby crystal clear.

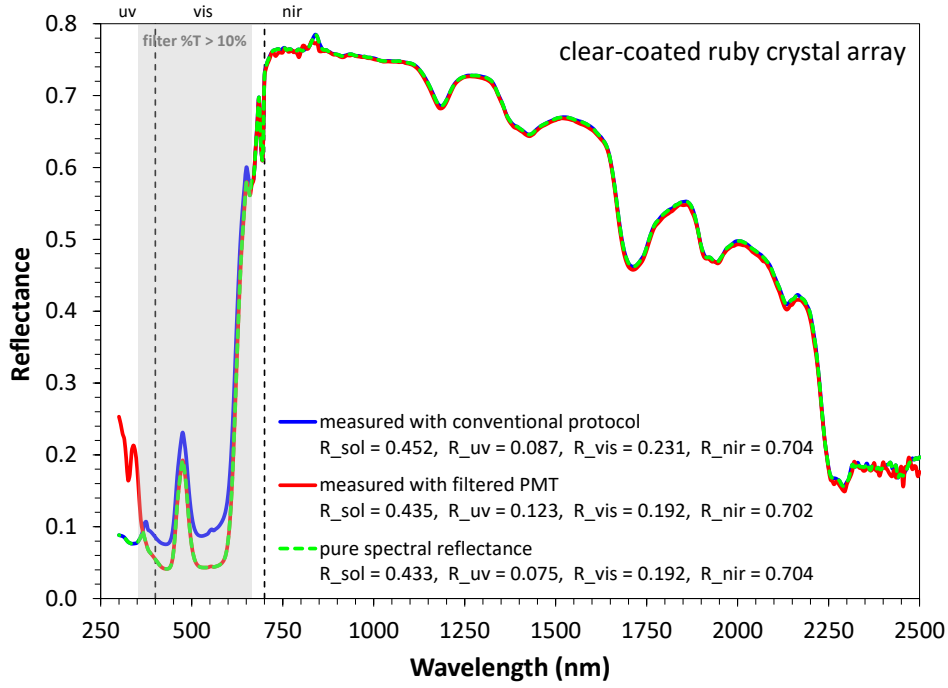

Figure 6. Solar spectral “effective” reflectance (blue curve, measured without correction) and solar spectral reflectance (red curve, measured by filtering emission) of ruby crystal clear. Pure spectral reflectance (red curve) replaces filtered data with non-filtered data where filter transmittance exceeds 10%. Each spectrum was obtained with a UV-VIS-NIR spectrophotometer with integrating sphere. The effective reflectance spectrum will be inaccurate if instrument response at emission wavelengths differs from that at excitation wavelengths.

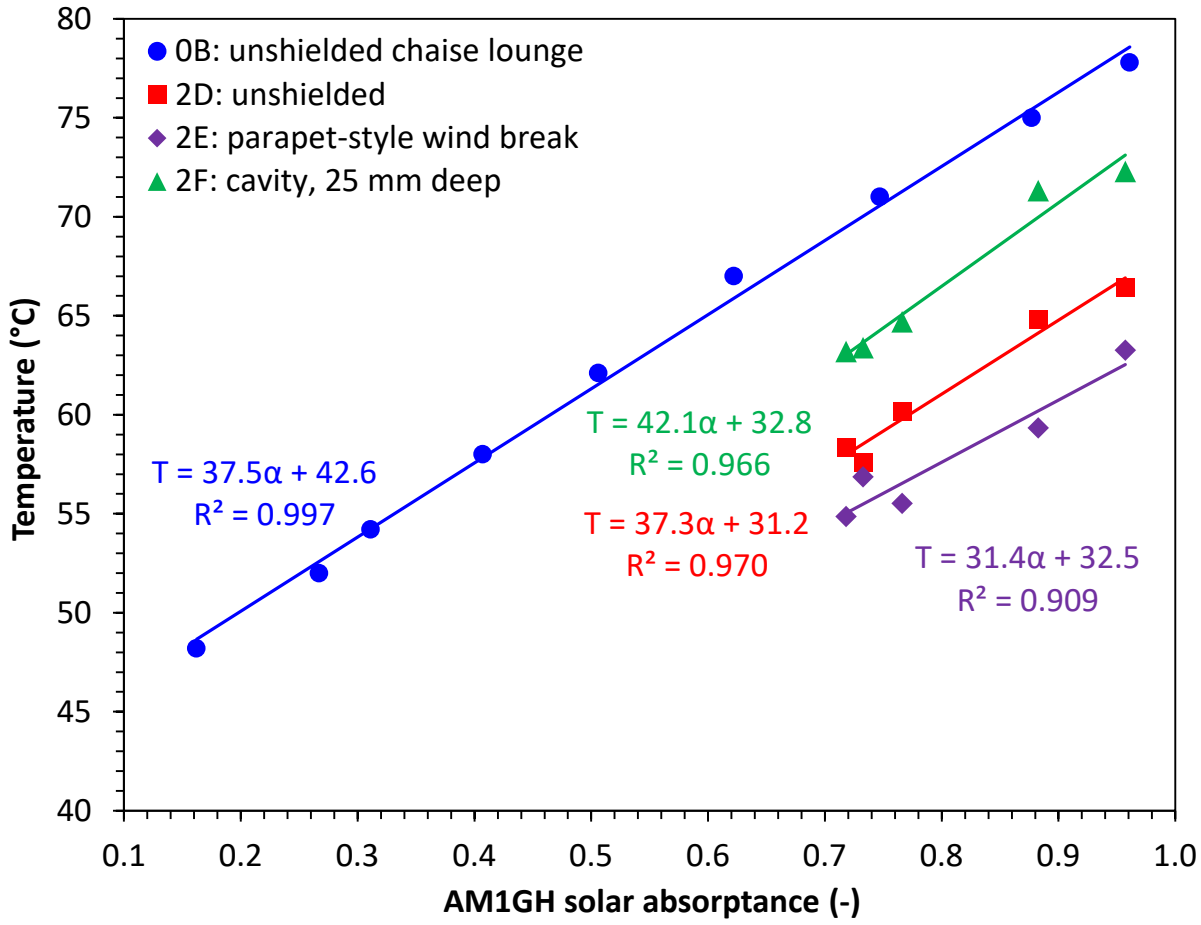

Figure 7. In experiment 0B, the median surface temperatures of nine non-fluorescent painted metal panels (reference specimens A1 – A9) varied nearly linearly with solar absorptance on a sunny, calm afternoon in July 2015. Also shown are variation of time-averaged surface temperature with solar absorptance of non-fluorescent specimens tested in Experiment 2, trials 2D – 2F, conducted on sunny days in October 2015.

Figure 8. Three-cavity insulated apparatus used to measure the ESA of the ruby crystal test specimen (center cavity). Image also shows the pyranometer and anemometer used to measure solar irradiance and wind speed.

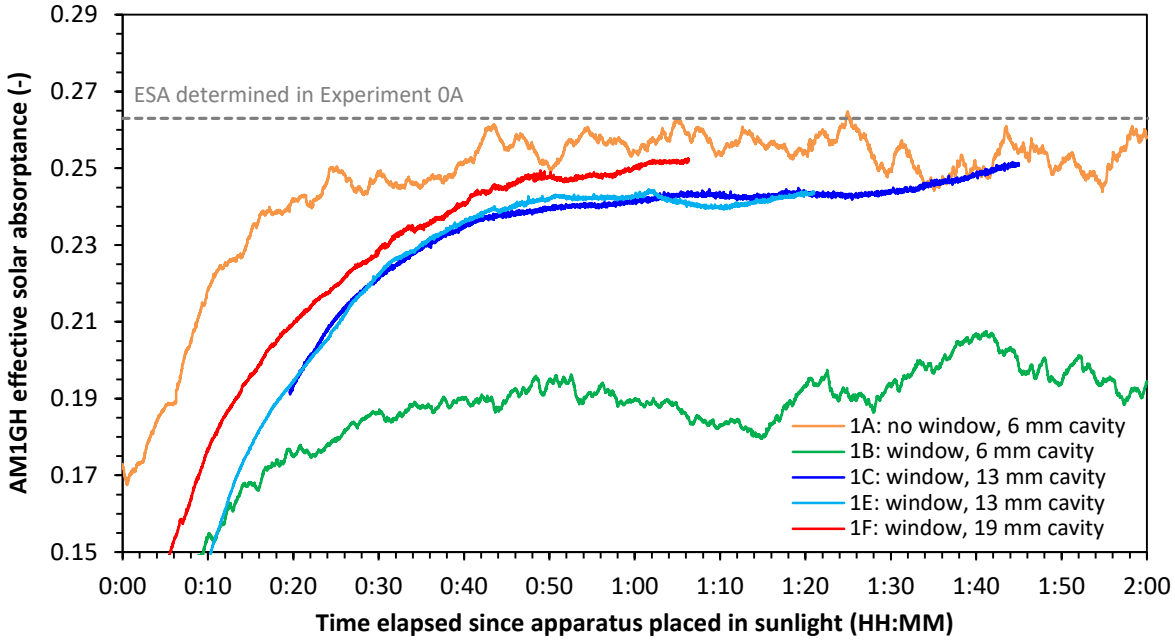

673

674 Figure 9. Effective solar absorptance of ruby crystal test specimen interpolated from solar
675 absorptances of gray#2 (A3) and white (A1) reference specimens, using temperatures
676 measured with several versions of the Experiment 1 apparatus.

677

678

(a)

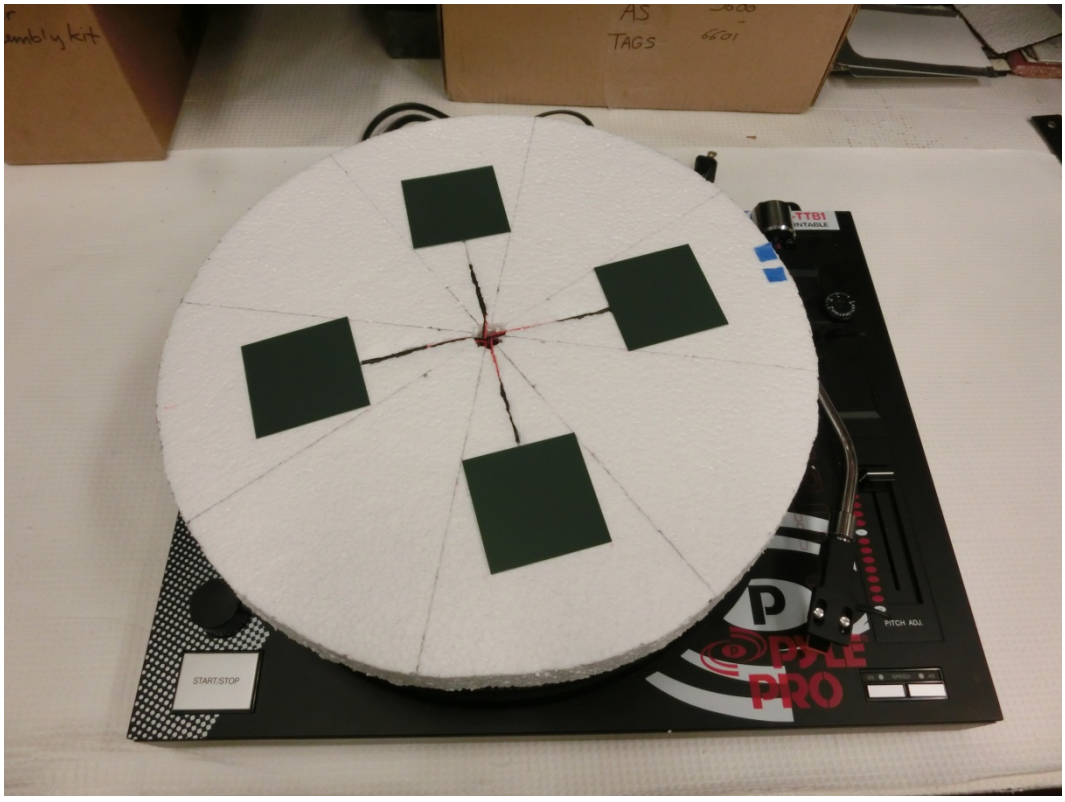

(b)

Figure 10. Images of a continuously rotating platform on a phonographic turntable, including (a) a top view showing four duplicate coupons, and (b) a look under the hood. The four specimens are spaced 5 cm from each other, and 3.8 cm from the platform edge.

679

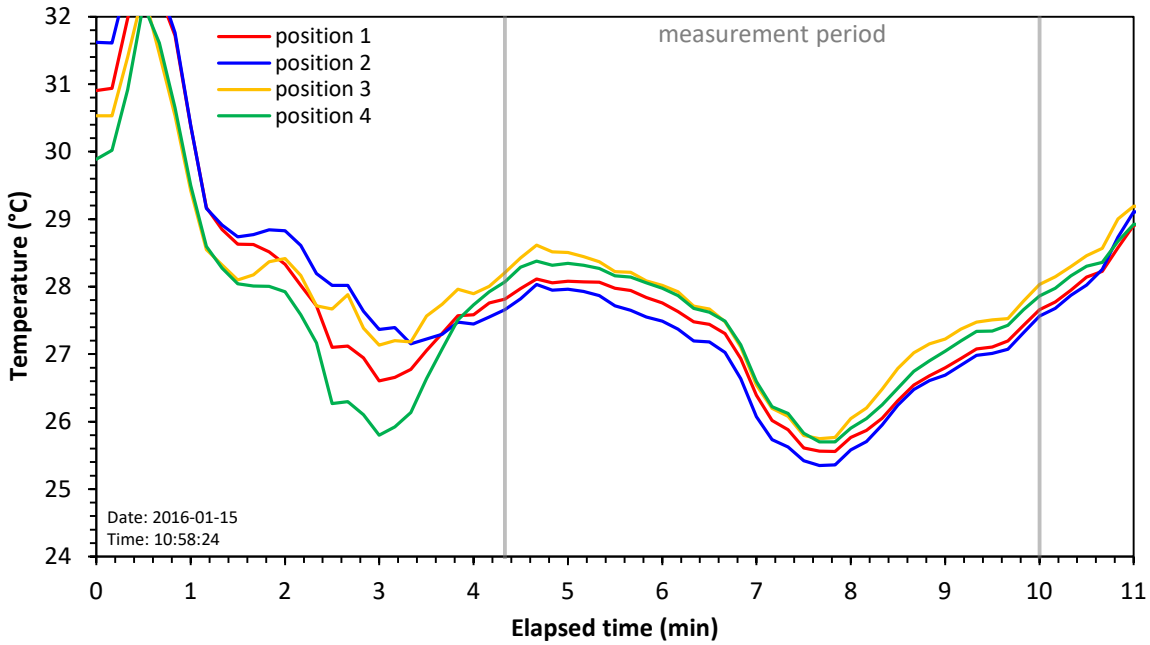

Figure 11. Surface temperatures of duplicate non-fluorescent specimens measured on a platform revolving at 33 RPM, measured in trial 3C of Experiment 3. Outside air temperature was about 18 °C.

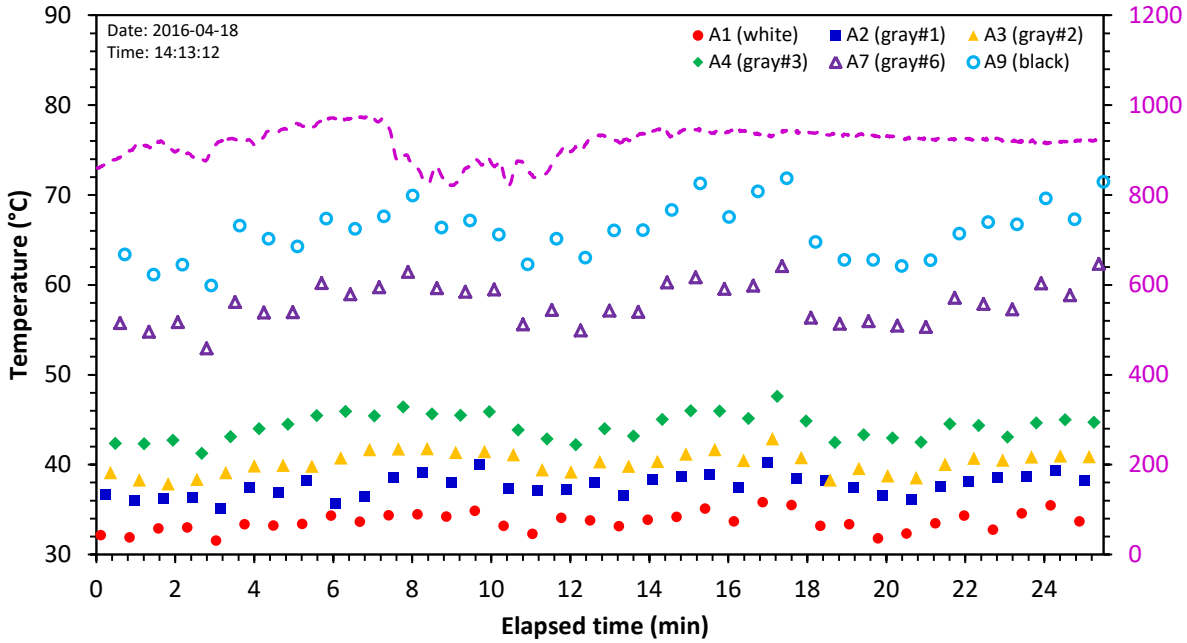

Figure 12. Instantaneous surface temperatures of six gray-scale reference specimens measured with the initial programmable rotary apparatus in trial 4D. Also shown is global horizontal solar irradiance.

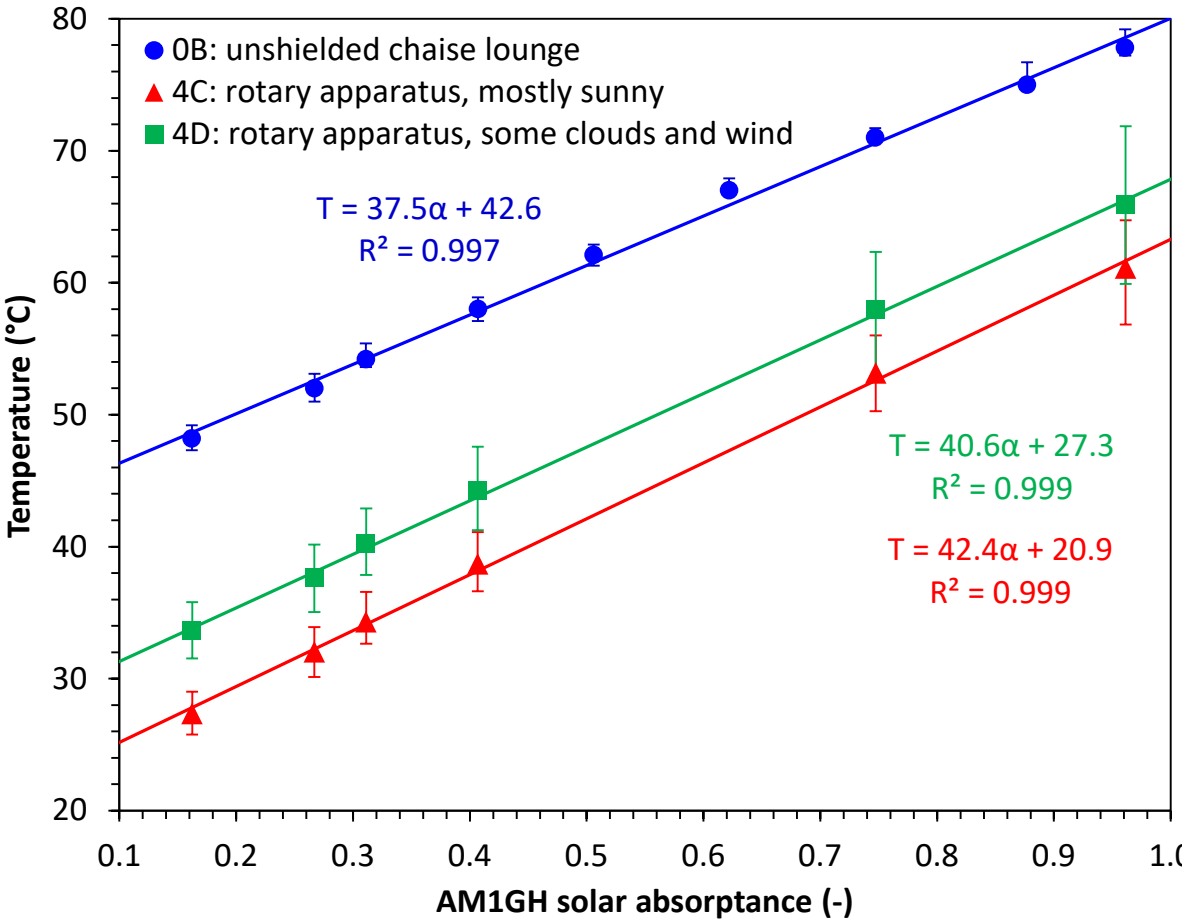

Figure 13. Variation with solar absorptance of the time-averaged temperatures of six gray-scale reference specimens (L to R: A1, A2, A3, A4, A7, and A9) measured with the initial programmable rotary apparatus in Trials 4C and 4D (April 2016). Also shown for comparison are the temperatures of all nine gray-scale reference specimens (L to R: A1 – A9) in Trial 0B (June 2015). Error bars bound low and high values.

Figure 14. Photo of final apparatus, including rotating platter, IR thermometer (upper right), anemometer (lower left), pyranometer (on same board as anemometer), and control electronics (underneath tripod). The air temperature sensor is hidden below the platter.

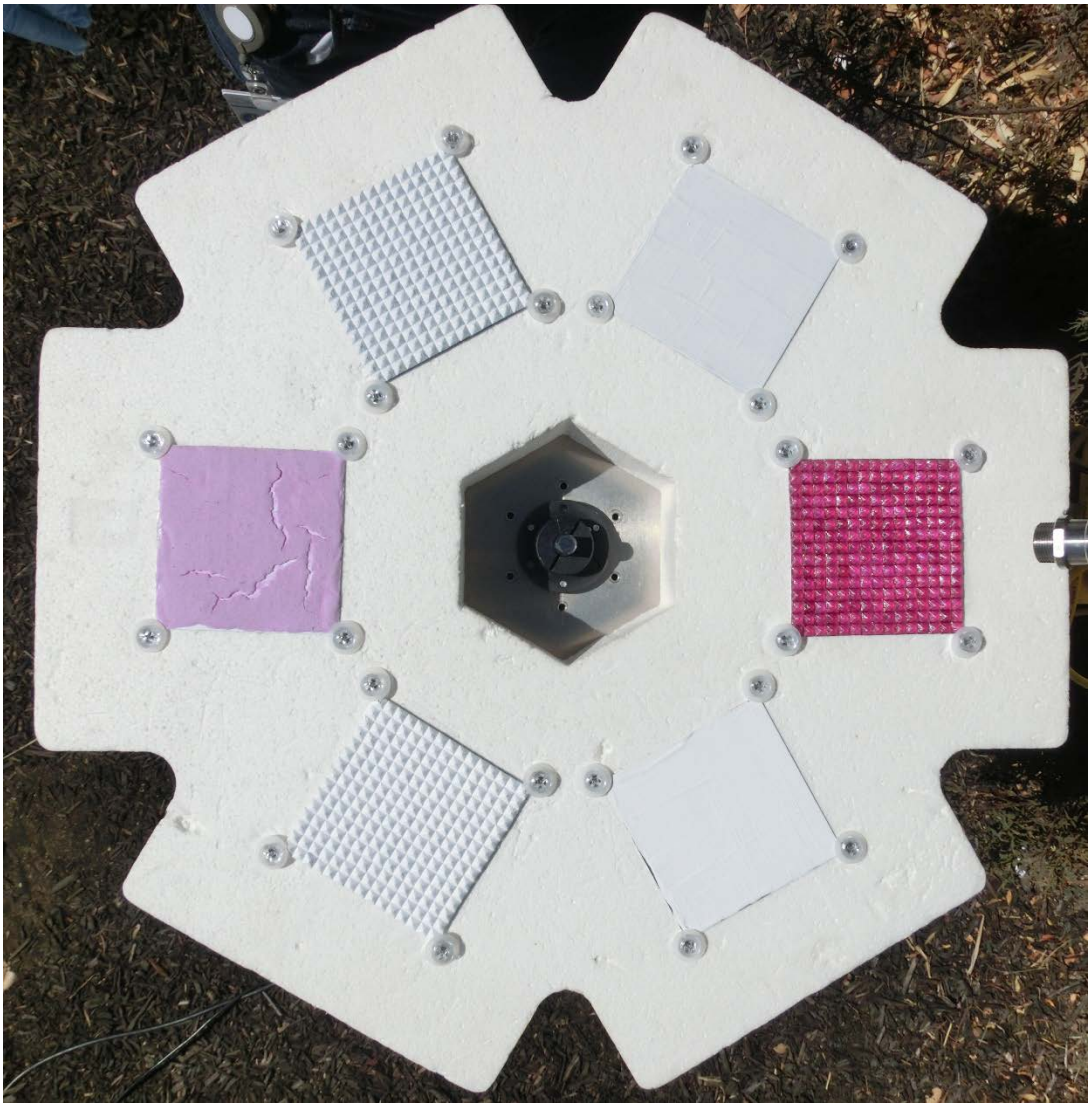

Figure 15. Top view of Set D on the platter. Clockwise from left: 2% coating, ruby crystal gray, A2 (gray#1), ruby crystal clear, A1 (white), and ruby crystal white.

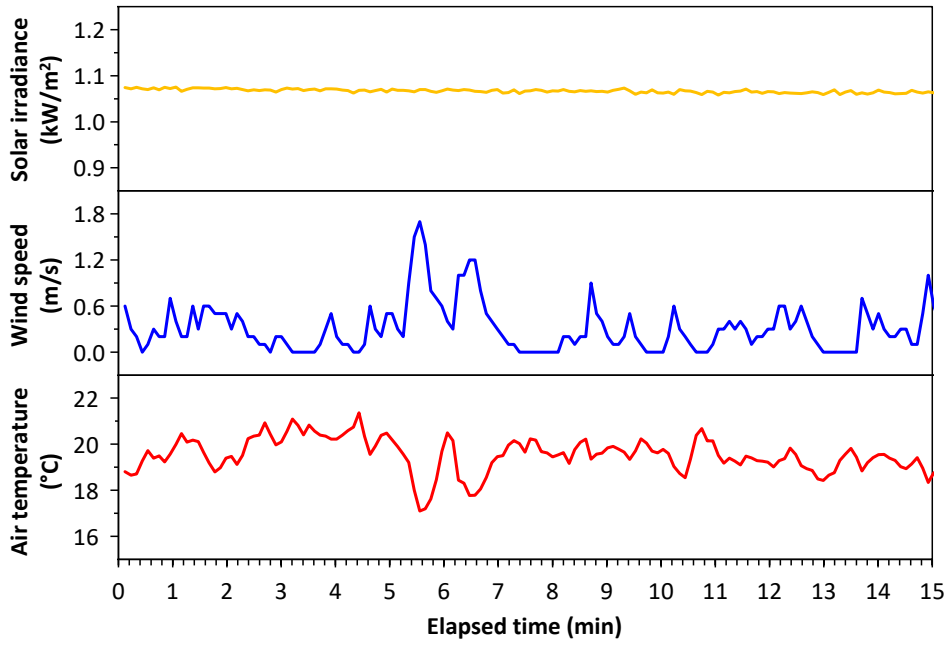

(a)

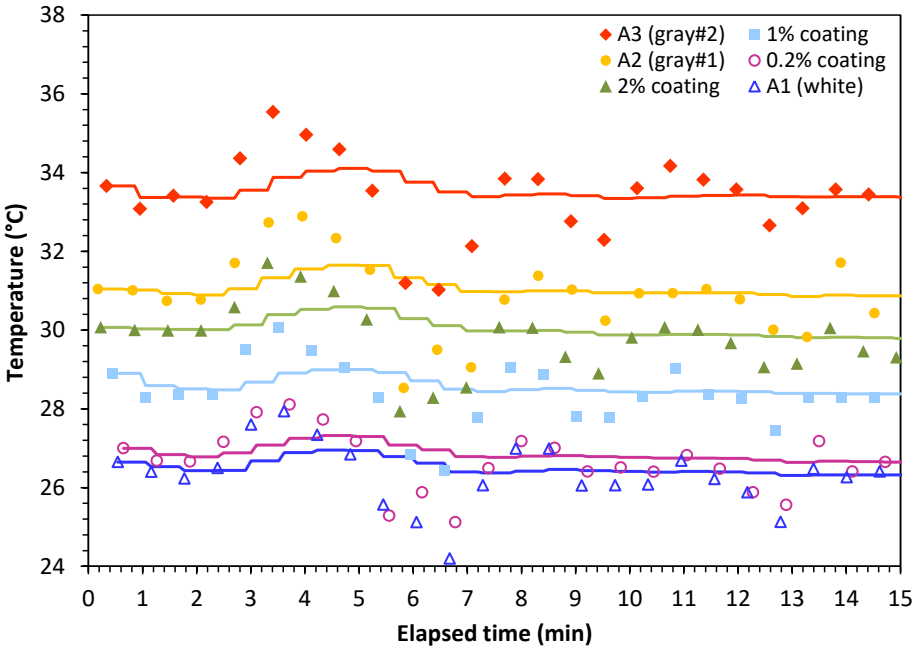

(b)

Figure 16. Time series of (a) weather and (b) specimen temperatures measured during Trial 5C. In panel b, symbols are instantaneous values and lines are cumulative means.

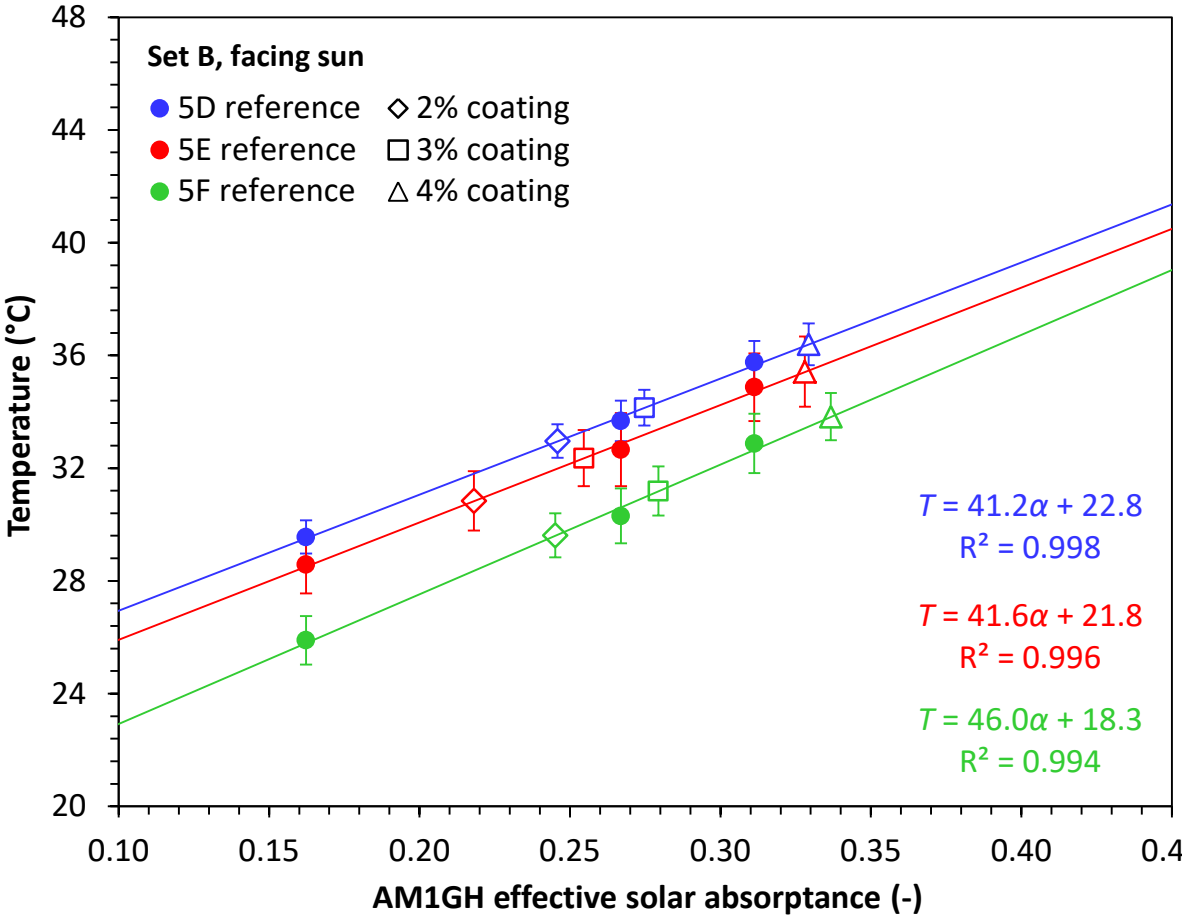

Figure 17. Determination of test specimen ESA from final mean temperatures of test and reference specimens, shown for trials 5D – 5F (Set B, facing sun).

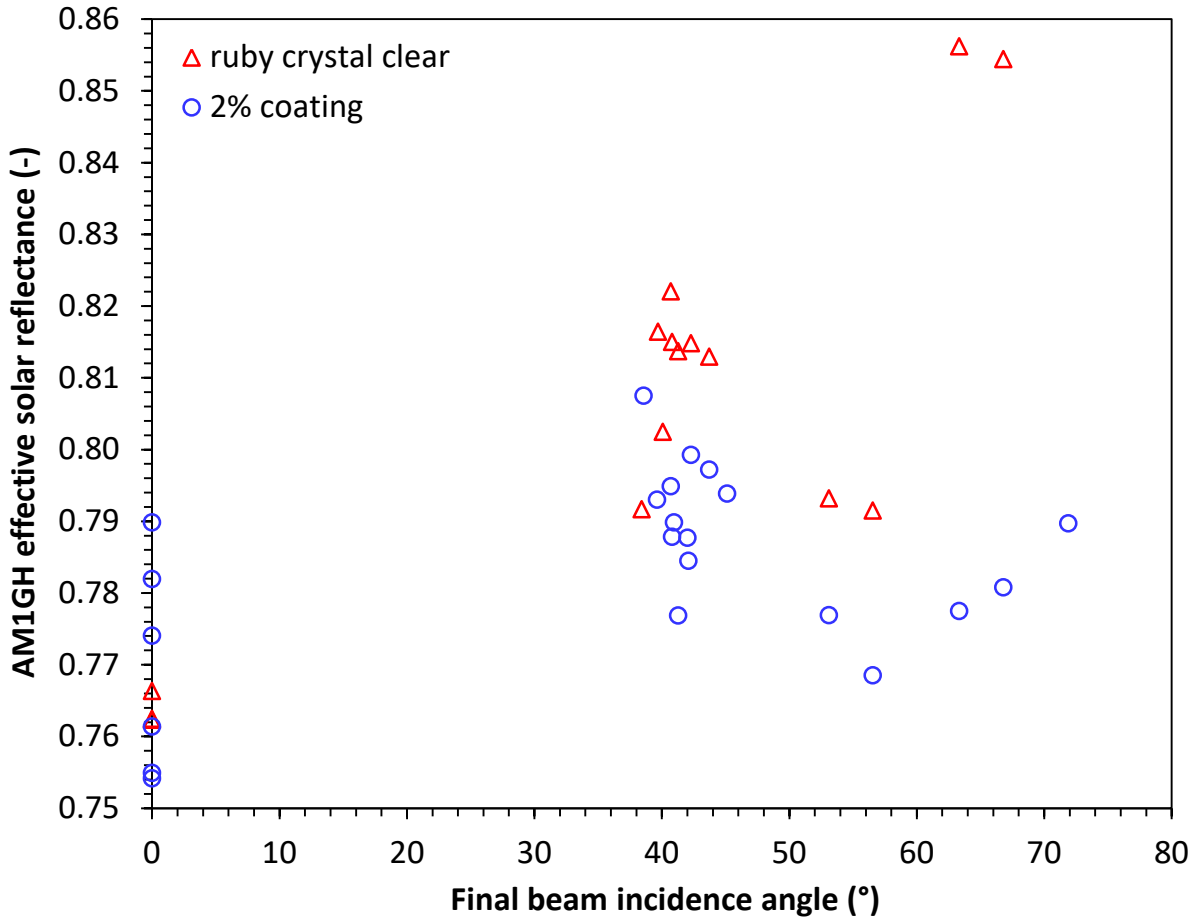

680

681 Figure 18. Variation of ESR with solar beam incidence angle for 2% ruby coating and ruby
682 crystal clear.
683

684 Table 1. Radiative properties of fluorescent test specimens.

Description	Specimen thickness (mm)	Thermal emittance	Pure AM1GH solar reflectance w/o window
0.2% coating	1.4	0.885	0.732
1% coating	1.6	0.876	0.679
2% coating	1.6	0.880	0.640
3% coating	1.7	0.884	0.626
4% coating	1.6	0.885	0.588
ruby crystal clear	4	0.875	0.434

685

686 Table 2. Radiative properties of non-fluorescent reference specimens, including solar
687 reflectances measured without and with a quartz window over the spectrophotometer's
688 reflectance port. Each specimen is 75 mm by 75 mm.

Code	Description	Coating dry film thickness (μm)	Specimen thickness (mm)	Thermal emittance	AM1GH solar reflectance w/o window	AM1GH solar reflectance w/ window
A1	white	120	1.1	0.888	0.838	0.762
A2	gray #1	108	1.1	0.888	0.733	0.665
A3	gray #2	169	1.2	0.895	0.689	0.615
A4	gray #3	248	1.2	0.886	0.593	0.547
A5	gray #4	214	1.2	0.900	0.494	0.463
A6	gray #5	214	1.2	0.897	0.378	0.366
A7	gray #6	174	1.2	0.905	0.253	0.264
A8	gray #7	217	1.2	0.918	0.123	0.165
A9	black	106	1.1	0.926	0.039	0.102
A10	ruby crystal white		4	0.911	0.769	
A11	ruby crystal gray		4	0.912	0.638	

689
690

691

692 Table 3. Conditions and outcomes of Trials in Experiment 5 (i/iii).

693

Trial	5A	5B	5C	5D	5E	5F	5G	5H	5I
specimen set	A	A	A	B	B	B	C	C	C
specimen orientation [a]	FS	FS	FS	FS	FS	FS	FS	FS	FS
date (2016-MM-DD)	09-27	09-28	09-28	09-27	09-28	09-28	09-27	09-27	09-28
measurement start (LDT)	13:43	12:35	15:17	17:34	12:00	16:21	14:36	15:51	13:16
spin-up time (min)	10	10	10	10	10	10	10	10	10
measurement time (min)	15.5	15.5	15.3	15.3	15.6	15.5	15.5	15.4	15.7
measurement revolutions	25	25	25	25	25	25	25	25	25
initial solar elevation (°)	48.8	49.3	38.6	15.3	47.5	28.5	44.2	33.7	49.5
final solar elevation (°)	47.8	49.7	36.4	12.4	48.5	25.8	42.3	31.2	49.0
final beam incidence angle (°)	0	0	0	0	0	0	0	0	0
mean solar irradiance (kW/m^2)	1.063	1.049	1.067	0.862	1.043	0.984	0.976	0.920	1.069
s.d.	0.009	0.004	0.004	0.019	0.003	0.007	0.145	0.129	0.003
mean wind speed (m/s)	0.16	0.33	0.31	0.00	0.22	0.14	0.11	0.02	0.27
s.d.	0.17	0.22	0.32	0.02	0.15	0.14	0.18	0.06	0.21
mean air temperature (°C)	27.8	19.1	19.5	24.7	19.4	18.4	32.5	32.8	19.5
s.d.	0.49	0.89	0.77	0.35	0.96	0.66	2.94	0.79	0.81
ruby crystal clear ESR							0.762	0.766	0.762
0.2% coating ESR	0.826	0.824	0.829						
1% coating ESR	0.838	0.825	0.792						
2% coating ESR	0.790	0.774	0.761	0.754	0.782	0.755			
3% coating ESR				0.725	0.745	0.721			
4% coating ESR				0.671	0.672	0.663			

694 [a] FS = facing sun; H = horizontal.
695

696 Table 3 (continued, ii/iii).

697

Trial	5J	5K	5L	5M	5N	5O	5P	5Q	5R
specimen set	A	A	A	B	B	B	C	C	C
specimen orientation [a]	H	H	H	H	H	H	H	H	H
date (2016-MM-DD)	09-21	09-24	09-26	09-22	09-26	09-27	09-23	09-26	09-27
measurement start (LDT)	14:16	11:17	12:32	11:59	13:31	11:46	12:38	13:01	12:28
spin-up time (min)	10	10	10	10	10	10	10	10	10
measurement time (min)	33.5	32.7	15.5	32.7	15.5	15.3	33.0	15.4	15.5
measurement revolutions	50	50	25	50	25	25	50	25	25
initial solar elevation (°)	48.6	44.6	50.0	49.4	49.8	46.7	51.3	50.5	49.5
final solar elevation (°)	44.9	48.0	50.4	51.4	49.0	47.9	51.6	50.3	49.9
final beam incidence angle (°)	45.1	42.0	39.6	38.6	41.0	42.1	38.4	39.7	40.1
mean solar irradiance (kW/m^2)	0.807	0.783	0.861	0.895	0.819	0.906	0.876	0.861	0.895
s.d.	0.040	0.015	0.003	0.008	0.042	0.004	0.003	0.003	0.010
mean wind speed (m/s)	0.33	0.14	0.25	0.36	0.16	0.02	0.36	0.22	0.08
s.d.	0.33	0.19	0.25	0.33	0.22	0.07	0.33	0.25	0.11
mean air temperature (°C)	21.5	24.6	32.7	20.3	33.6	28.3	22.4	33.5	28.6
s.d.	1.21	0.86	0.82	1.16	0.83	0.78	0.99	0.76	0.62
ruby crystal clear ESR							0.792	0.816	0.802
0.2% coating ESR	0.851	0.854	0.861						
1% coating ESR	0.844	0.841	0.838						
2% coating ESR	0.794	0.788	0.793	0.807	0.790	0.784			
3% coating ESR				0.776	0.761	0.747			
4% coating ESR				0.704	0.682	0.683			

698

699

700 Table 3 (continued, iii/iii).

Trial	5S/i	5S/ii	5S/iii	5S/iv	5S/v	5S/vi	5S/vii	5S/viii	5S/ix	5S/x	5T	5U
specimen set	D	D	D	D	D	D	D	D	D	D	E	E
specimen orientation [a]	H	H	H	H	H	H	H	H	H	H	FS	H
date (2016-MM-DD)	09-29	09-29	09-29	09-29	09-29	09-29	09-29	09-29	09-29	09-29	09-28	09-26
measurement start (LDT)	12:38	12:56	13:13	13:33	13:52	15:10	15:33	16:13	16:33	17:00	14:10	10:56
spin-up time (min)	10	1	1	1	1	10	1	10	1	5	10	10
measurement time (min)	15.7	15.7	15.7	15.7	15.8	15.7	15.7	15.7	15.6	16.3	15.4	9.5
measurement revolutions	25	25	25	25	25	25	25	25	25	25	25	15
initial solar elevation (°)	49.1	49.3	49.2	48.6	47.5	39.2	35.9	29.4	26.0	21.1	46.5	41.4
final solar elevation (°)	49.3	49.2	48.7	47.7	46.3	36.9	33.5	26.7	23.2	18.1	45.0	42.6
final beam incidence angle (°)	40.7	40.8	41.3	42.3	43.7	53.1	56.6	63.3	66.8	71.9	0	47.4
mean solar irradiance (kW/m^2)	0.850	0.853	0.848	0.833	0.814	0.649	0.584	0.534	0.468	0.322	1.043	0.759
s.d.	0.003	0.003	0.003	0.005	0.006	0.011	0.014	0.014	0.016	0.055	0.003	0.005
mean wind speed (m/s)	0.20	0.12	0.18	0.13	0.14	0.24	0.17	0.16	0.07	0.16	0.16	0.28
s.d.	0.17	0.15	0.25	0.18	0.18	0.26	0.22	0.17	0.14	0.18	0.18	0.20
mean air temperature (°C)	18.0	18.6	18.6	18.4	18.2	19.4	19.2	19.0	19.7	17.9	20.1	28.8
s.d.	1.16	1.26	1.34	1.21	1.09	1.42	1.04	1.16	0.89	0.84	0.84	0.51
ruby crystal clear ESR	0.822	0.815	0.814	0.815	0.813	0.793	0.792	0.856	0.854	0.910		
0.2% coating ESR												
1% coating ESR												
2% coating ESR	0.795	0.788	0.777	0.799	0.797	0.777	0.768	0.777	0.781	0.790		
3% coating ESR												
4% coating ESR												

701

702

Table 4. ESRs of fluorescent specimens by measurement orientation, showing sample count, mean, and standard deviation. Horizontal measurements include only those in which the final solar elevation angle was at least 40°. Also shown are pure SR and fluorescence benefit (ESR facing sun – pure SR).

effective solar reflectance	ESR facing sun			ESR horizontal			ESR horizontal – ESR facing sun	pure SR	fluorescence benefit (ESR facing sun – pure SR)
	count	mean	s.d.	count	mean	s.d.			
ruby crystal clear	3	0.764	0.002	8	0.811	0.010	0.047	0.434	0.330
0.2% coating	3	0.826	0.002	3	0.855	0.005	0.029	0.732	0.095
1% coating	3	0.818	0.023	3	0.841	0.003	0.023	0.679	0.140
2% coating	6	0.769	0.015	11	0.792	0.008	0.023	0.640	0.130
3% coating	3	0.730	0.013	3	0.761	0.015	0.031	0.626	0.104
4% coating	3	0.669	0.005	3	0.689	0.012	0.021	0.588	0.081

A. Electronic Supplementary Material

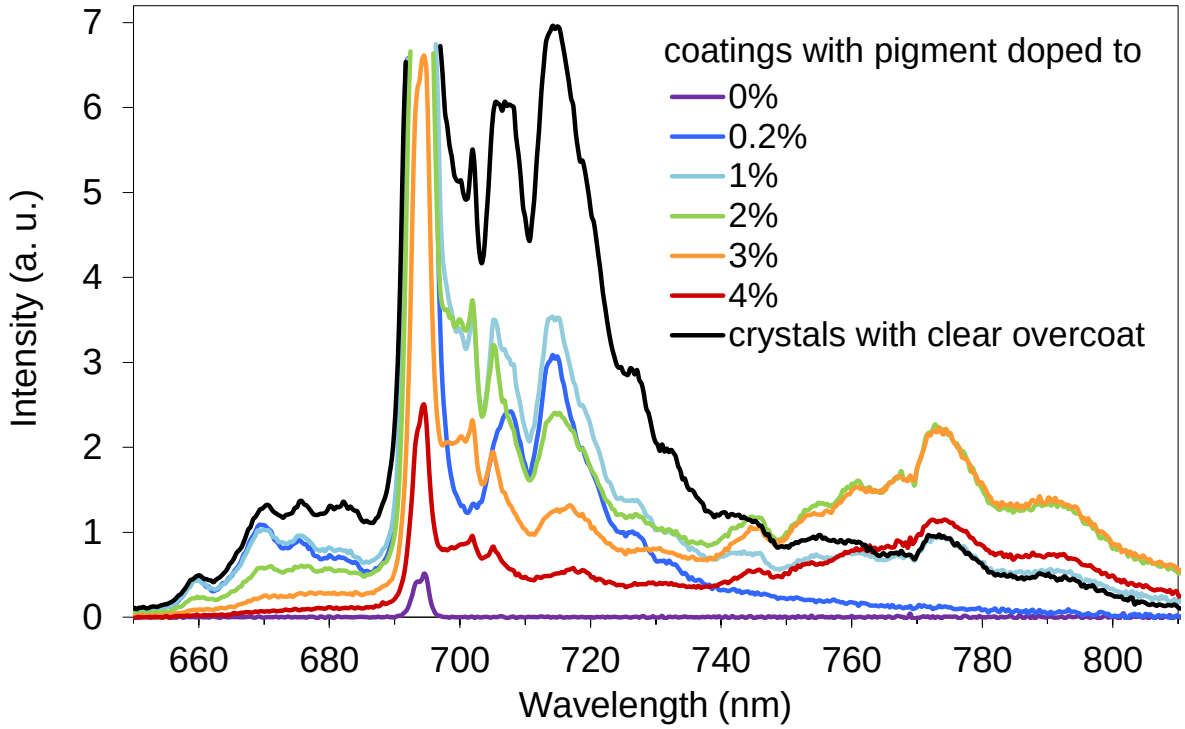

ESM Figure A-1. More detail of the spectra in Figure 5. Note that the nominal 0% pigment must contain a trace of Cr, since a double peak is visible near 694 nm.

(a) (b) (c)

ESM Figure A-2. Photomultiplier tube sensor (250 – 900 nm) in the integrating sphere of a UV-VIS-NIR spectrophotometer (a) exposed and (b) covered with a removable filter. The filter (c) is mounted in a paper cup that has been painted bright white. It passes 90 to 95% of light from 400 to 650 nm, and reflects nearly 100% of light from 650 to 865 nm.

ESM Figure A-3. Reclining chair with towel used to support specimens in Experiment 0. Note that this photo shows a set of specimens different from that used in Experiment 0.

(a)

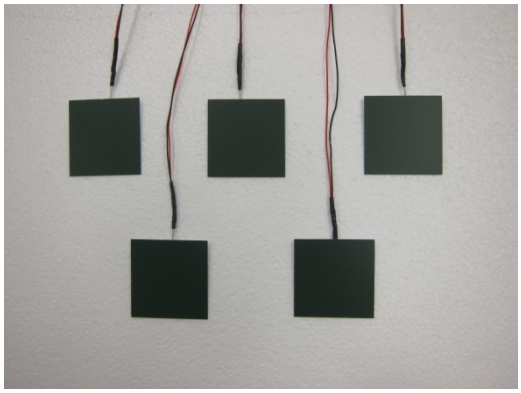

(b)

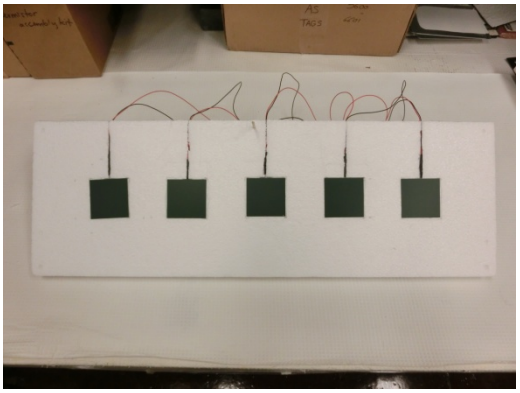

(c)

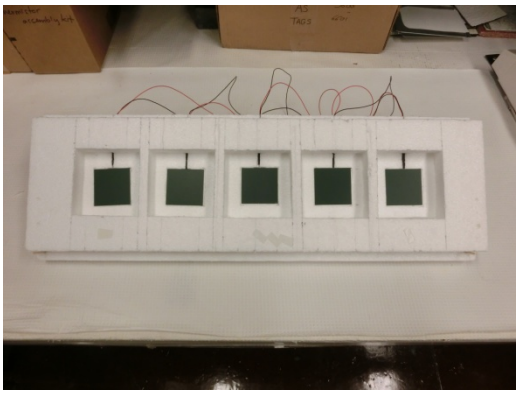

(d)

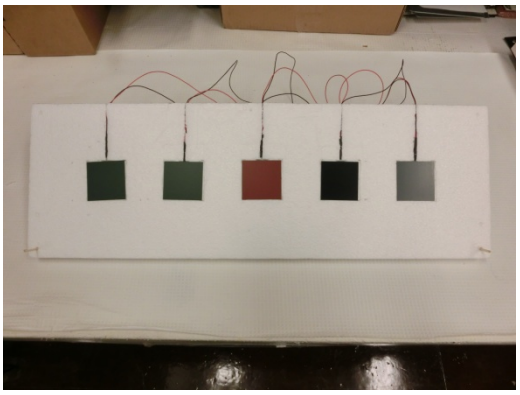

(e)

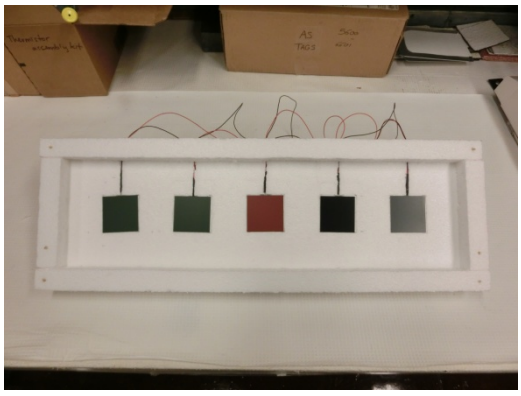

(f)

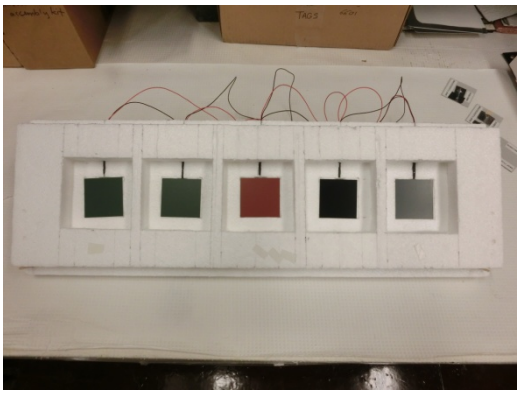

ESM Figure A-4. Apparata and specimens (50 mm by 50 mm) used in Experiment 2, including (a) trial 2A, five duplicate specimens arranged in two rows at the center of a 36 cm by 38 cm by 2.5 cm foam board; (b) trial 2B, the five duplicates arranged in one row on a 20 cm by 61 cm by 2.5 cm foam board; (c) trial 2C, the five duplicates in a cavity array (9 cm by 9 cm, 25 mm deep); (d) trial 2D, five different specimens exposed as in 2B; (e) trial 2E, adding a parapet-style wind break (25 mm height, 5 cm from the specimen row) to the 2D setup; and (f) trial 2F, five different specimens exposed as in 2C.

725

726

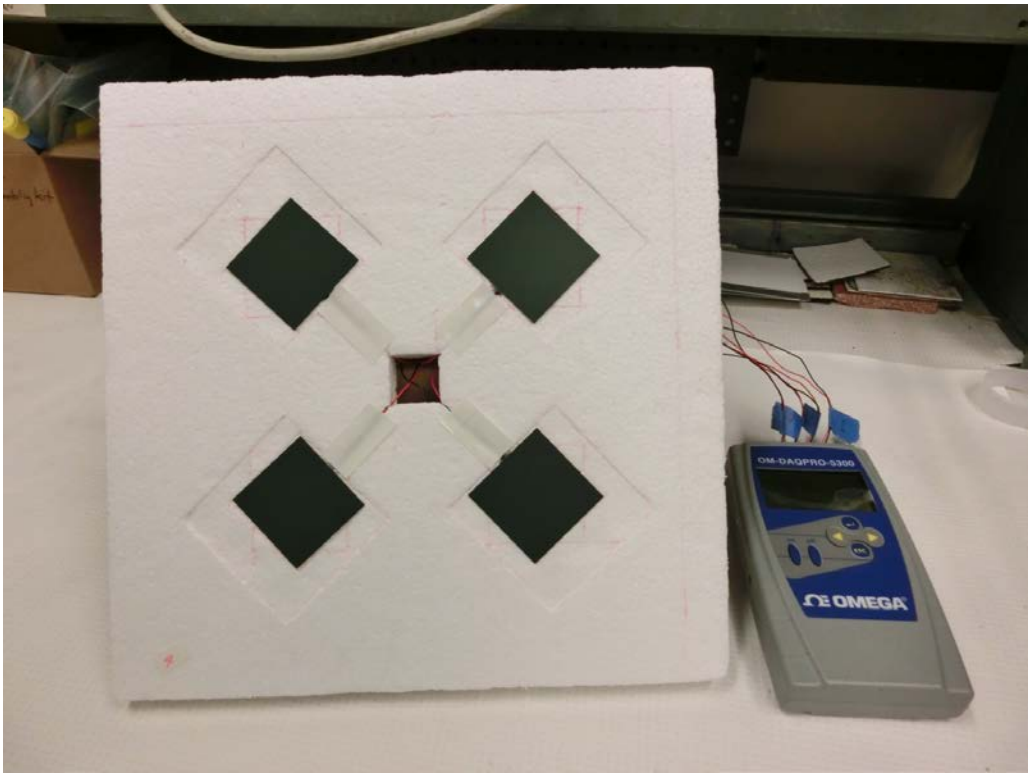

ESM Figure A-5. Duplicate non-fluorescent specimens on a manually rotated platform with four very shallow cavities. The specimens are arranged in a two by two array on a 33 by 33 by 2.5 cm foam board, with 5 cm spacing. The margin on each side is 6.4 cm.

732

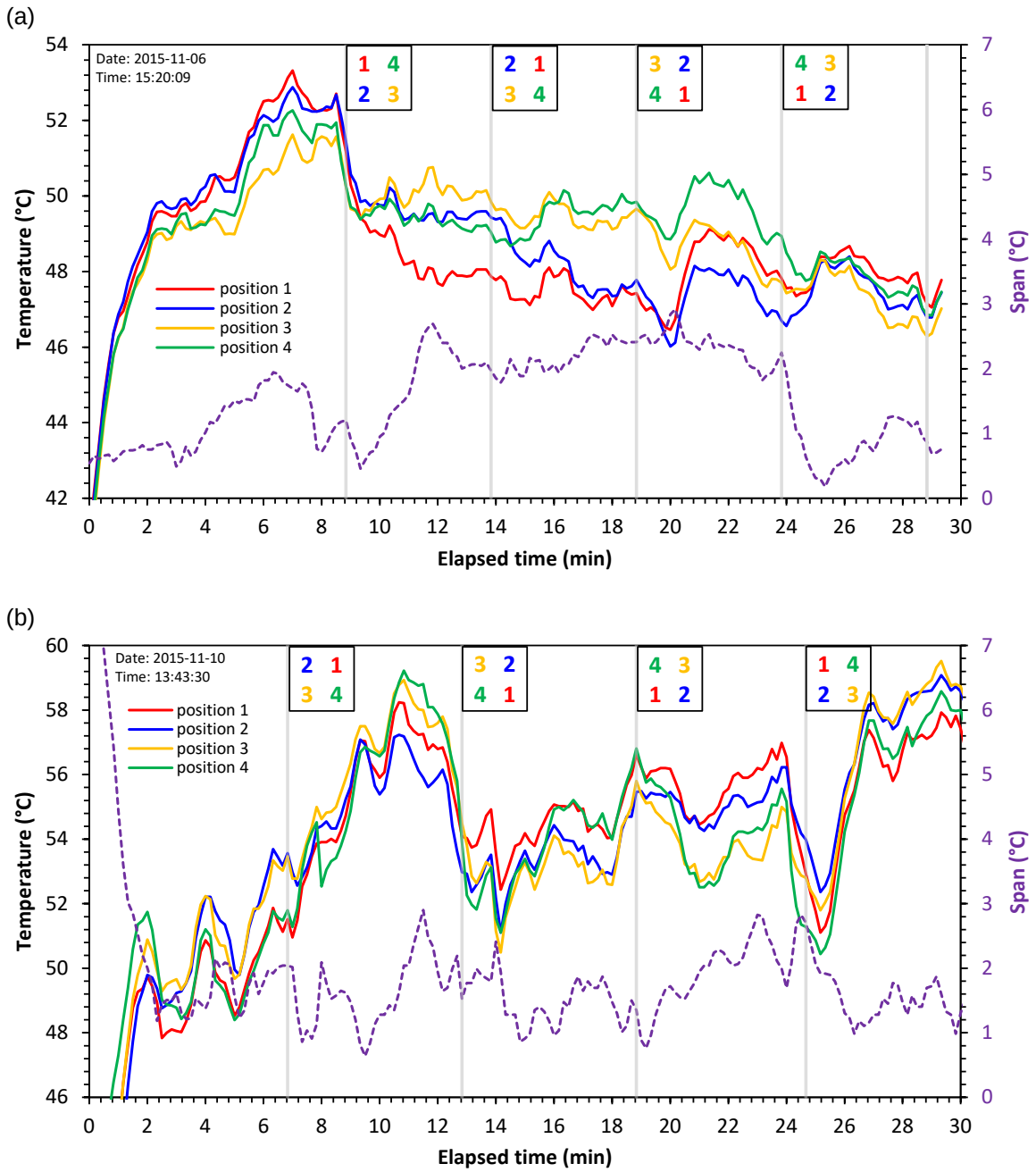

ESM Figure A-6. Surface temperatures and surface temperature range of duplicate non-fluorescent specimens measured on a manually rotated platform, measured in (a) trial 3A and (b) trial 3B of Experiment 3.

733

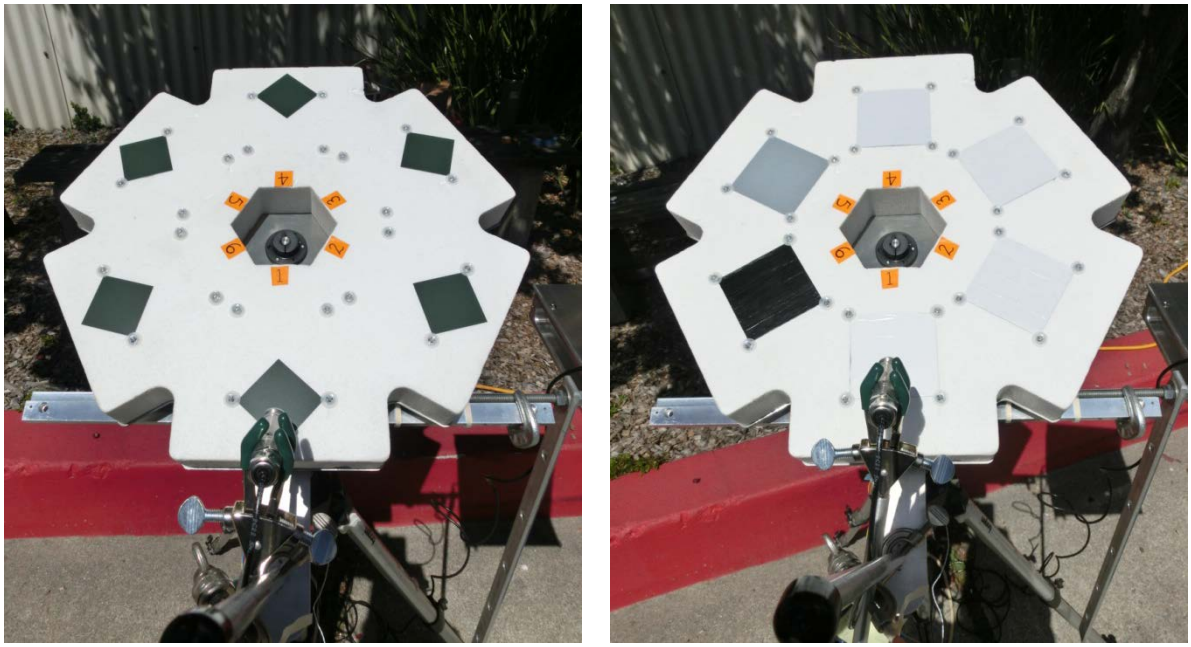

(a) (b)

ESM Figure A-7. Images of the initial programmable rotary apparatus configured for (a) trials 4A and 4B (six duplicate green specimens) and (b) trials 4C and 4D (six gray-scale reference specimens). The fixed-position infrared thermometer is shown in foreground.

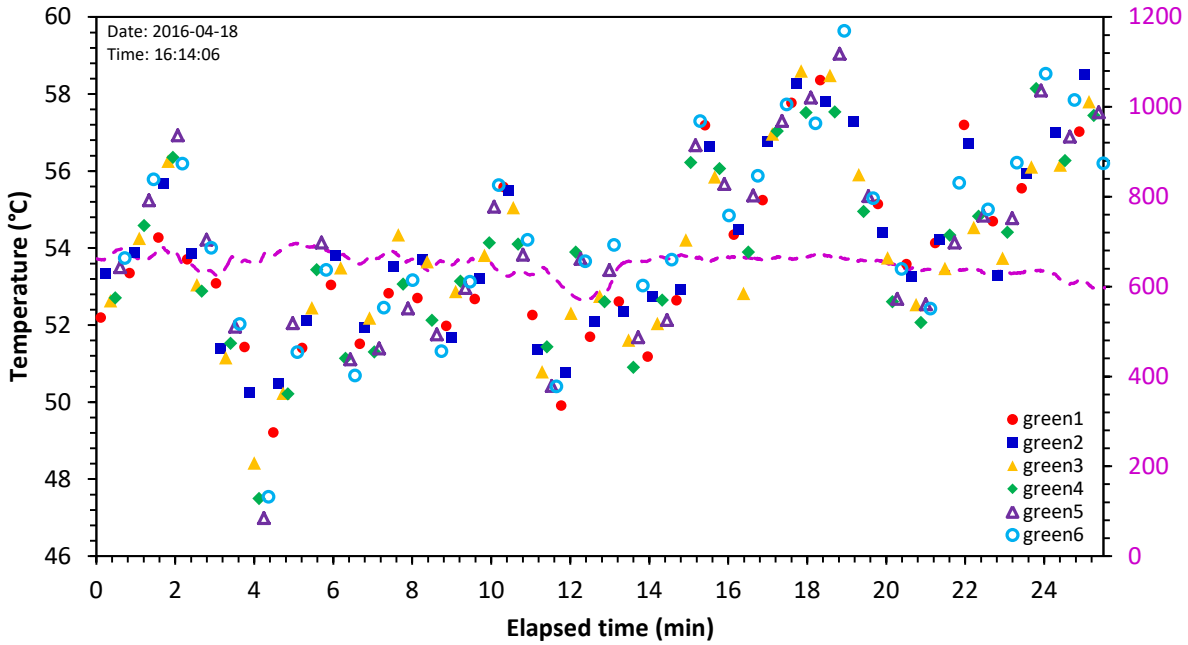

ESM Figure A-8. Instantaneous surface temperatures of six duplicate green specimens measured with the initial programmable rotary apparatus in trial 4B. Also shown is global horizontal solar irradiance.

734

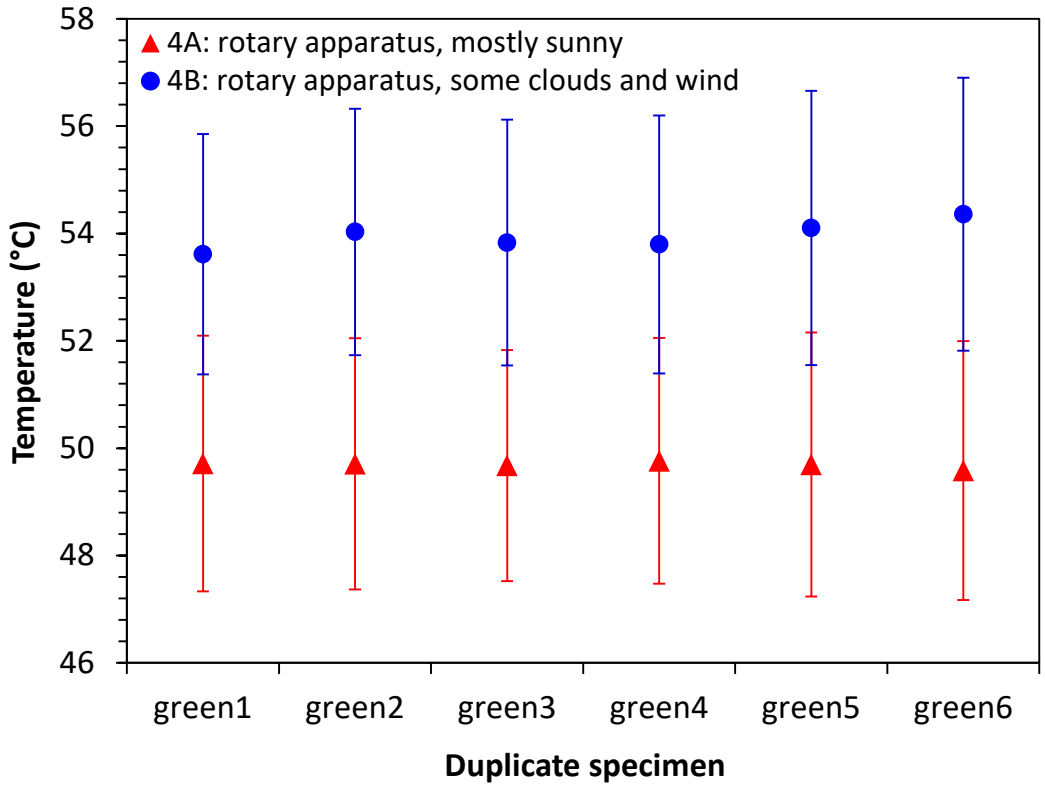

ESM Figure A-9. Means and standard deviations of duplicate green specimen temperatures measured with the initial programmable rotary apparatus in trials 4A and 4B.

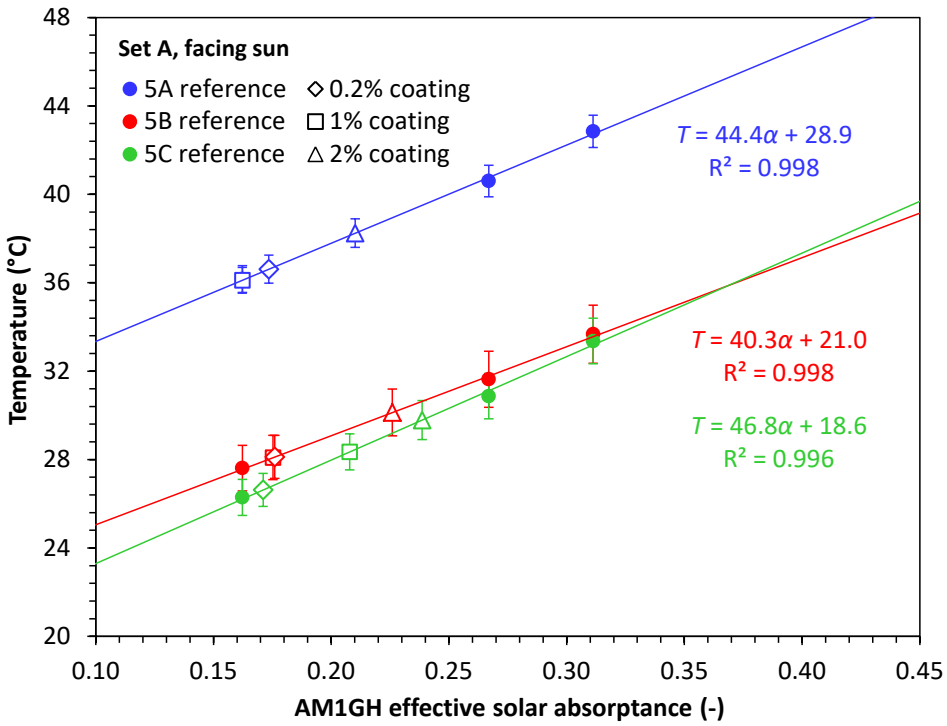

(a)

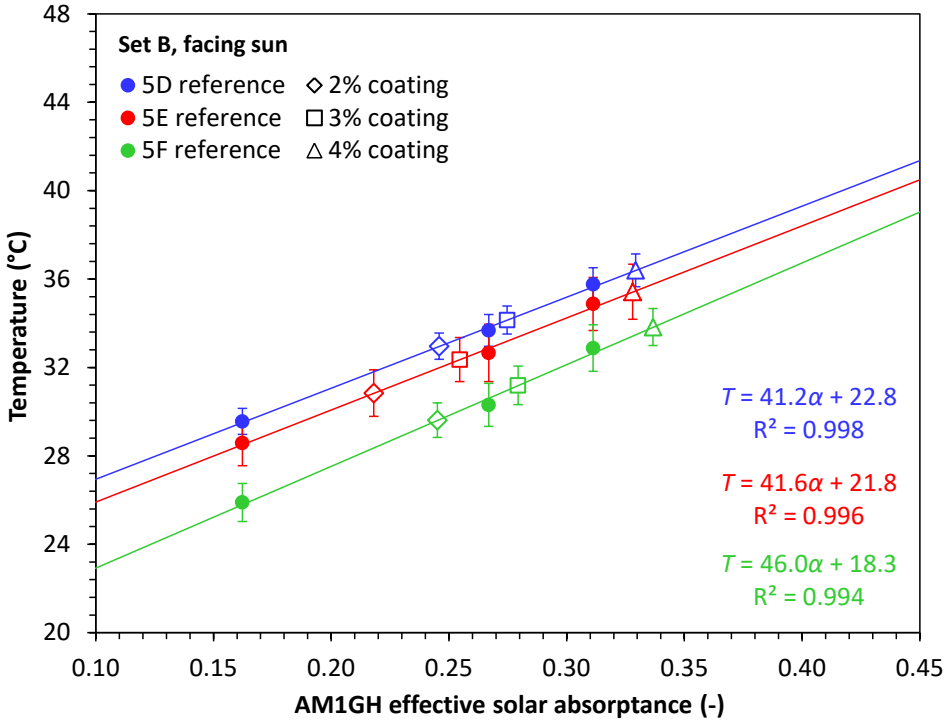

(b)

ESM Figure A-10. Determination of test specimen ESA from final mean temperatures of test and reference specimens, shown for (a) trials 5A – 5C (Set A, facing sun); (b) trials 5D – 5F (Set B, facing sun); (c) trials 5G – 5I (Set C, facing sun); (d) trials 5J – 5L (Set A, horizontal); (e) trials 5M – 5O (Set B, horizontal); and (f) trials 5P – 5R (Set C, horizontal. Note that trial 5M used reference A4 (gray#3) in place of reference A3 (gray#2).

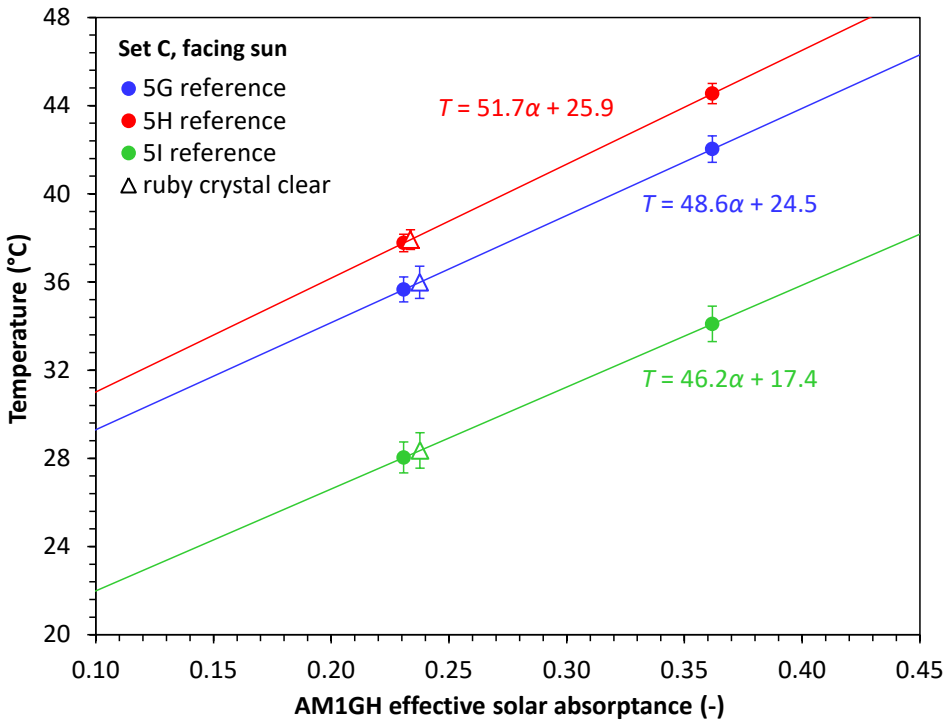

(c)

ESM Figure A-10 (continued)

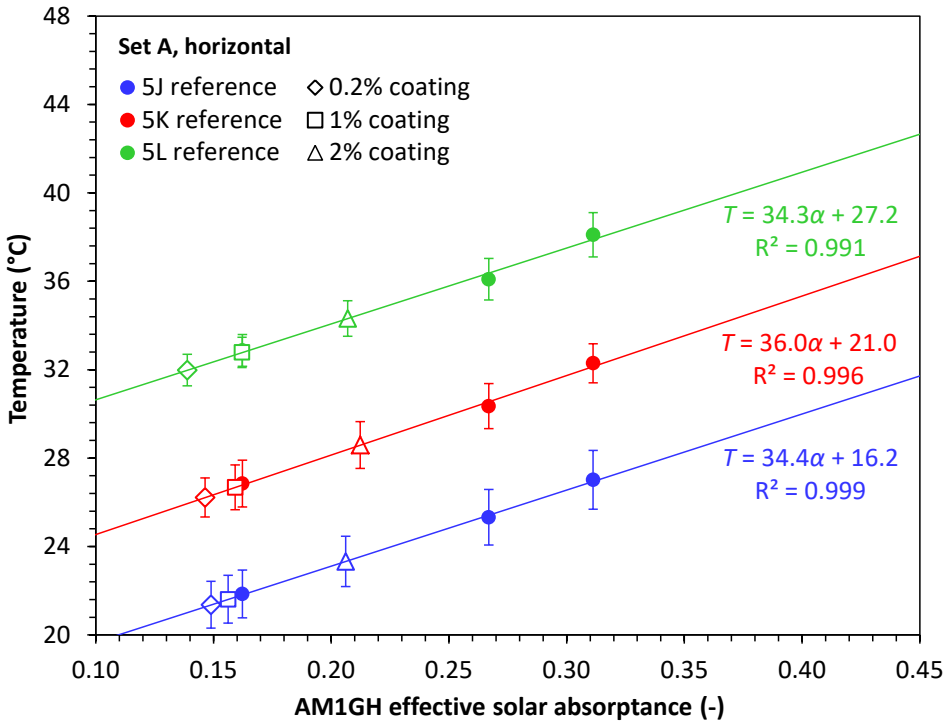

(d)

ESM Figure A-10 (continued)

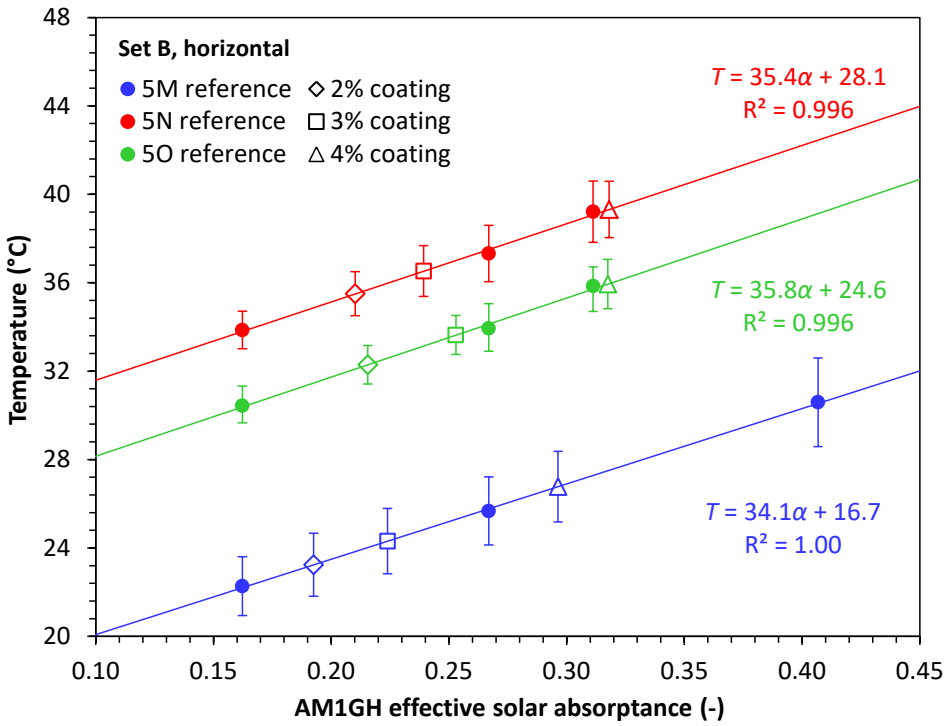

(e)

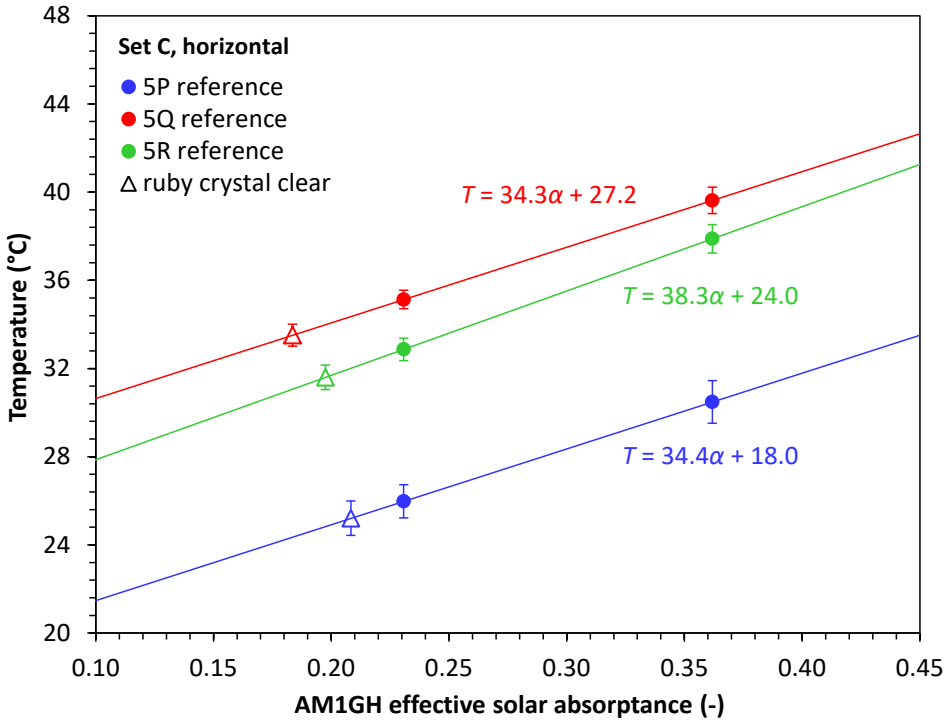

(f)

ESM Figure A-10 (continued)

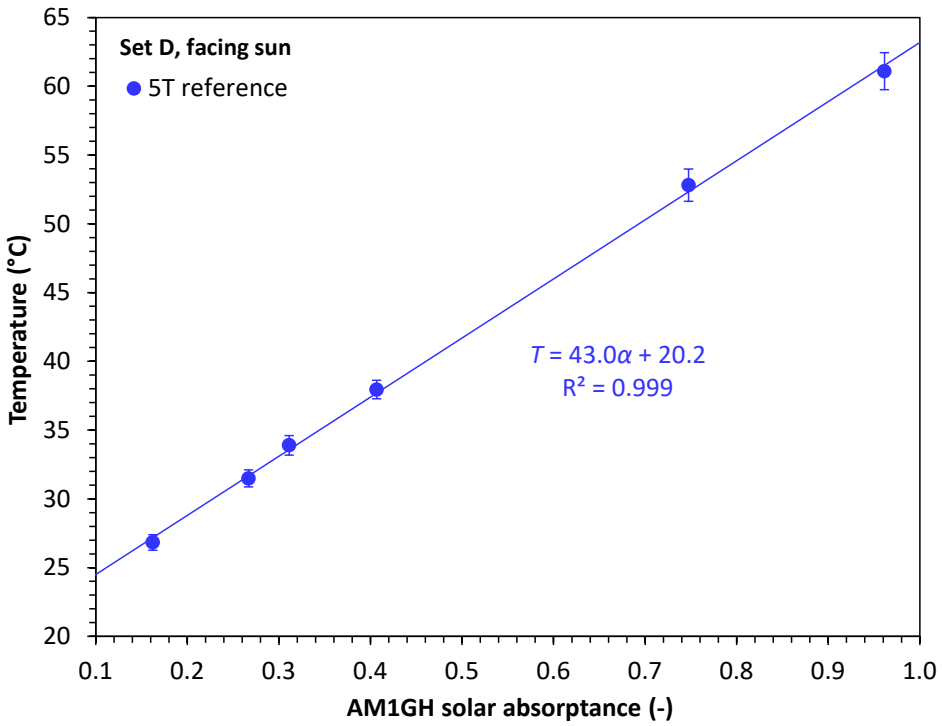

(a)

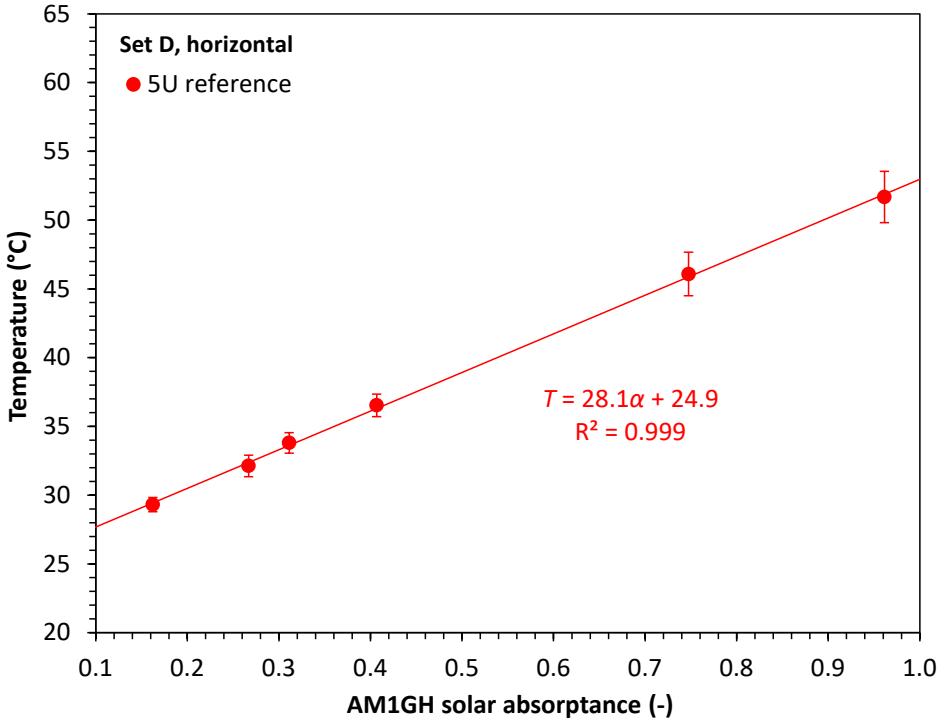

(b)

ESM Figure A-11. Final mean temperature versus pure SA for non-fluorescent reference specimens, shown for (a) trial 5T (Set E, facing sun) and (b) trial 5U (Set E, horizontal).

767 ESM Table A-1. Measurement sensors and protocols used in calorimetric experiments.

	Experiment 0A	**Experiment 0B**	**Experiment 1**	**Experiment 2**	**Experiment 3**	**Experiment 4**	**Experiment 5 (final apparatus)**
Specimen surface temperature							
Sensor type	Thermistor, NTC 10K ohm	Handheld infrared thermometer	Thermistor, NTC 10K ohm	Thermistor, NTC 10K ohm	Thermistor, NTC 10K ohm	Fixed-mount infrared thermometer	Same as Experiment 4
Sensor make and model	Omega 44006	VWR Traceable Infrared Thermometer (Cat. No. 36934-178)	Omega 44006	US Sensor PR103J2	US Sensor PR103J2	Omega OS151-MT	Same as Experiment 4
Sensor range	-80 to 120 °C	-60 to 500 °C	-80 to 120 °C	-55 to 80 °C	-55 to 80 °C	0 to 250°C	Same as Experiment 4
Sensor accuracy (nominal)	unknown	±(2% + 1 °C) %	unknown	±0.05 °C	±0.05 °C	±1% of reading or ±1°C, whichever is greater	Same as Experiment 4
Sensor repeatability (nominal)	unknown	unknown	unknown	unknown	unknown	±0.5% of reading or ±0.5°C, whichever is greater	Same as Experiment 4
Sensor interchangeability	±0.2 °C (0 to 70 °C)	—	±0.2 °C (0 to 70 °C)	±0.05 °C (0 to 50 °C)	±0.05 °C (0 to 50 °C)	unknown	Same as Experiment 4
Sensor features	—	adjustable emissivity	—	—	—	15:1 field of view; emissivity fixed at 0.95	Same as Experiment 4

	Experiment 0A	**Experiment 0B**	**Experiment 1**	**Experiment 2**	**Experiment 3**	**Experiment 4**	**Experiment 5 (final apparatus)**
Protocol	Sensors attached to back of specimen with aluminum tape; 9 measurements logged over a period of 11 min	Instrument held briefly above each of 9 specimens; 8 measurement sets performed over a period of 30 min	Sensor attached to back of specimen with thermal paste and aluminum tape; measurements logged every 1 sec over a period of 1-2 hrs	Sensor attached to back of specimen with thermal paste and aluminum tape; measurements logged every 10 sec over a period of 20 min	Sensor attached to back of specimen with thermal paste and aluminum tape; measurements logged every 10 sec over a period of 20 min (3A and 3B) or 6 min (3C)	To reduce shadows, sensor mounted ~3.8 cm from center of specimen, with 55-65° angle between sensor axis and specimen plane; waited 4-5 sec for reading to stabilize	Sensor mounted 2.5 cm (along line of sight) from center of specimen, with 45° angle between sensor axis and specimen plane.
Ambient air temperature							
Sensor type	Old-style bulb thermometer	Same as Experiment 0A	Thermistor, NTC 10K ohm	Same as Experiment 1	Same as Experiment 1	None	Thermistor, NTC 10K ohm
Sensor make and model	-	-	Omega 44006	Same as Experiment 1	Same as Experiment 1		US Sensor KS103G2
Sensor range	-30 to 50 °C	Same as Experiment 0A	-80 to 120 °C	Same as Experiment 1	Same as Experiment 1		-80 to 135 °C
Sensor accuracy	± 0.5 °C	Same as Experiment 0A	Unknown	Same as Experiment 1	Same as Experiment 1		see interchangeability
Sensor interchangeability	—	—	±0.2 °C (0 to 70 °C)	Same as Experiment 1	Same as Experiment 1		±0.1 °C (0 to 70 °C)
Sensor features	—		—	—	—		

	Experiment 0A	**Experiment 0B**	**Experiment 1**	**Experiment 2**	**Experiment 3**	**Experiment 4**	**Experiment 5 (final apparatus)**
Protocol	Measurements before and after experiment. Sensor in shade, height 1.5 m	Measurements before, at midpoint, and after experiment. Sensor in shade, height 1.5 m	Sensor installed on the back side of apparatus; measurements logged every 1 sec over a period of 1-2 hrs	Sensor installed on the back side of apparatus; measurements logged every 10 sec over a period of 20 min	Sensor installed on the back side of apparatus; measurements logged every 10 sec over a period of 20 min (3A and 3B) or 6 min (3C)		Sensor mounted on the underside of the specimen platter, shaded from sunlight.
Solar irradiance							
Sensor type	None	None	Silicon pyranometer	Same as Experiment 1	None	Same as Experiment 1	Same as Experiment 1
Sensor make and model			Kipp & Zonen SP Lite2	Same as Experiment 1		Same as Experiment 1	Same as Experiment 1
Sensor spectral range			400 to 1100 nm	Same as Experiment 1		Same as Experiment 1	Same as Experiment 1
Sensor max irradiance			2000 W/m²	Same as Experiment 1		Same as Experiment 1	Same as Experiment 1
Sensor accuracy			Unknown	Same as Experiment 1		Same as Experiment 1	Same as Experiment 1
Protocol			Sensor mounted on the front face of apparatus; measurements logged every 1 sec over a period of 1-2 hrs	Sensor placed immediately adjacent to apparatus and tilted equivalently; measurements logged every 10 sec over a period of 20 min		Sensor placed within 2 m of apparatus, in horizontal plane	Sensor placed on the ground within 1 m of apparatus. Sensor orientation (horizontal or tilted facing the sun) for each trial matched that of the specimens.

	Experiment 0A	**Experiment 0B**	**Experiment 1**	**Experiment 2**	**Experiment 3**	**Experiment 4**	**Experiment 5 (final apparatus)**
Wind speed							
Sensor type	None	None	Handheld vane anemometer	None	None	None	3-cup anemometer
Sensor make and model			PCE Instruments Anemometer PCE-AM 81				Adafruit product 1733
Sensor range			0.4 to 30 m/s				0.5 to 32 m/s
Sensor accuracy			±3% full scale (<20 m/s); ±4% full scale (>20 m/s)				resolution 0.1 m/s; worst-case accuracy 1 m/s
Protocol	Low wind speed required. (A cloth on apparatus must not move.)	Low wind speed required. (A cloth on apparatus must not move.)	Sensor placed behind apparatus with propeller oriented for measuring airflow parallel to apparatus; recorded maximum wind speed over experiment duration				Sensor placed on the ground within 1 m of apparatus

	Experiment 0A	**Experiment 0B**	**Experiment 1**	**Experiment 2**	**Experiment 3**	**Experiment 4**	**Experiment 5 (final apparatus)**
Data acquisition system							
Instrument type	Portable handheld data logger	None (measurements recorded manually)	Portable handheld data logger	Portable handheld data logger	Portable handheld data logger	Portable handheld data logger	Multifunction data acquisition device with Python application programming interface
Instrument make and model	Omega OM-DAQPRO-5300		Omega OM-DAQPRO-5300	Omega OM-DAQPRO-5300	Omega OM-DAQPRO-5300	Omega OM-DAQPRO-5300	LabJack T7

768